iScience

CellPress

Article

Septin 9 has Two Polybasic Domains Critical to Septin Filament Assembly and Golgi Integrity

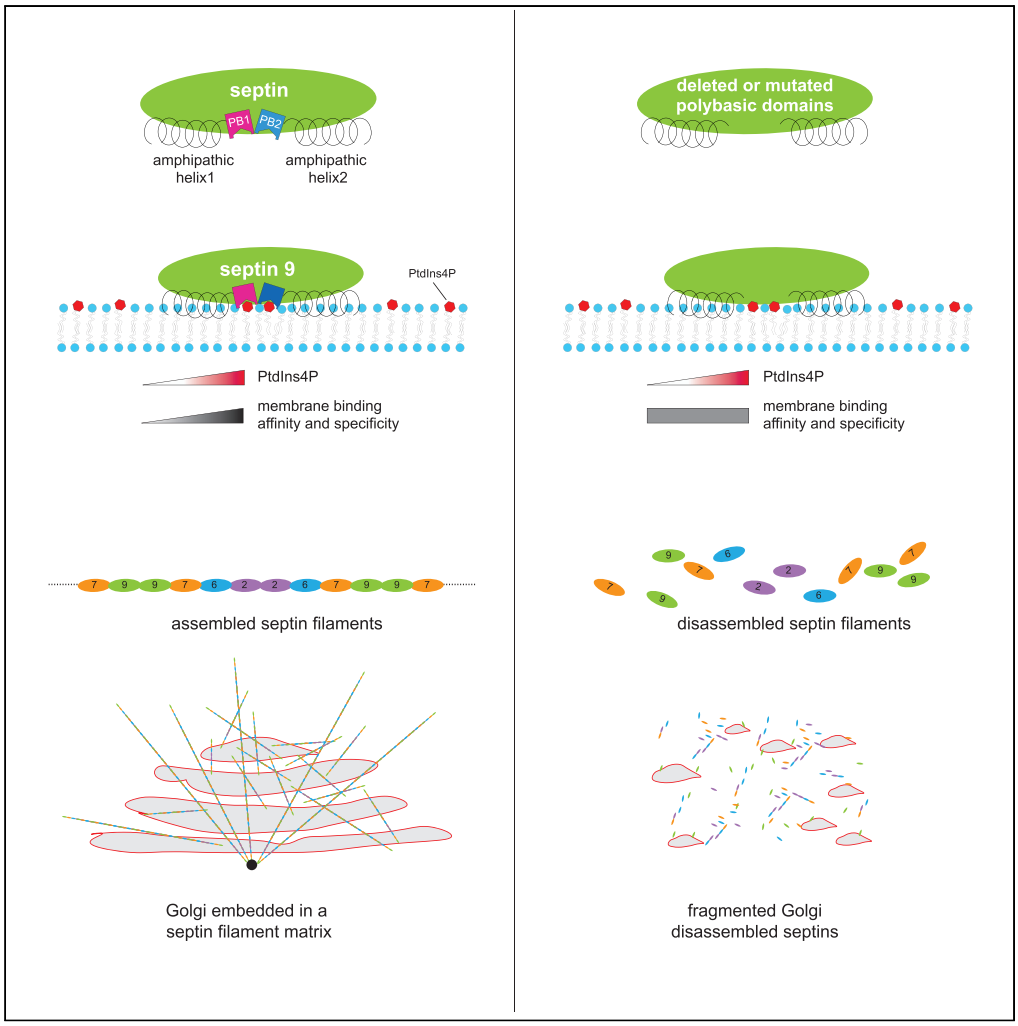

Mohyeddine Omrane, Amanda Souza Camara, Cyntia Taveneau, ..., Richard Charles Garratt, Abdou Rachid Thiam, Ama Gassama-Diagne

thiam@ens.fr (A.R.T.)
ama.gassama@inserm.fr (A.G.-D.)

HIGHLIGHTS

Two polybasic domains mediate septin 9 interactions with PIs

Human septins have amphipathic helices suitable for membrane binding

Septin 9 polybasic domains mediate the formation of septin higher-order structures

The mutation or depletion of septin polybasic domains induces Golgi fragmentation

Omrane et al., iScience *13*, 138–153
March 29, 2019
https://doi.org/10.1016/j.isci.2019.02.015

iScience

CellPress

Article

Septin 9 has Two Polybasic Domains Critical to Septin Filament Assembly and Golgi Integrity

Mohyeddine Omrane,[1,2,3] Amanda Souza Camara,[4] Cyntia Taveneau,[5] Nassima Benzoubir,[1,2] Thibault Tubiana,[5] Jinchao Yu,[5,6] Raphaël Guérois,[5,6] Didier Samuel,[1,2] Bruno Goud,[7] Christian Poüs,[1,2] Stéphane Bressanelli,[5] Richard Charles Garratt,[4] Abdou Rachid Thiam,[3,8,*] and Ama Gassama-Diagne[1,2,8,9,*]

SUMMARY

Septins are GTP-binding proteins involved in several membrane remodeling mechanisms. They associate with membranes, presumably using a polybasic domain (PB1) that interacts with phosphoinositides (PIs). Membrane-bound septins assemble into microscopic structures that regulate membrane shape. How septins interact with PIs and then assemble and shape membranes is poorly understood. Here, we found that septin 9 has a second polybasic domain (PB2) conserved in the human septin family. Similar to PB1, PB2 binds specifically to PIs, and both domains are critical for septin filament formation. However, septin 9 membrane association is not dependent on these PB domains, but on putative PB-adjacent amphipathic helices. The presence of PB domains guarantees protein enrichment in PI-contained membranes, which is critical for PI-enriched organelles. In particular, we found that septin 9 PB domains control the assembly and functionality of the Golgi apparatus. Our findings offer further insight into the role of septins in organelle morphology.

INTRODUCTION

Septins form a GTPase protein family that is found in eukaryotes from yeasts to animals but is absent in higher plants and certain protists (Pan et al., 2007; Nishihama et al., 2011). In mammals, 13 septins have been identified and placed in four classes (the septin 2, 3, 6, and 7 subgroups) (Peterson and Petty, 2010). Septins assemble into apolar complexes that are able to form higher-order structures such as filaments and rings (Weirich et al., 2008). Each septin has at least two interfaces: one interface contains GTP-binding domain motifs, referred to as the G interface, and the other contains the N and C termini of the protein, called the NC interface. Thus two septin proteins can develop G/G or NC/NC interactions with neighboring septins. Septins thereby form hetero-oligomeric complexes made up of hexameric subunits with the following sequence: (G7NC/NC6G/G2NC/NC2G/G6NC/NC7G) (Sirajuddin et al., 2007). Septin 9 assembles at the extremities of the hexamer to generate an octamer (Kim et al., 2011). This octamer has the NC interface of septin 9 at its ends, i.e., NC9G/G7NC/NC6G/G2NC/NC2G/G6NC/NC7G/G9NC, and is the building block for higher-order septin structures (Sirajuddin et al., 2007; Sellin et al., 2011; Kim et al., 2011). During membrane remodeling processes, these structures can act as a diffusion barrier or scaffold that recruits cytosolic proteins and other cytoskeletal elements such as microtubules or actins (Tanaka-Takiguchi et al., 2009; Fung et al., 2014; Bridges et al., 2016; Mostowy and Cossart, 2012).

Septins bind specifically to phosphoinositides (PIs) via a polybasic domain (PB1) located at the N terminus of their GTP-binding domain. This interaction with PIs supposedly mediates septin membrane association, which is a determining factor for the structural and functional features of the protein (Pan et al., 2007; Zhang et al., 1999; Tanaka-Takiguchi et al., 2009; Casamayor and Snyder, 2003). Septins associate with a variety of PIs at different intracellular membranes (Zhang et al., 1999; Akil et al., 2016; Dolat and Spiliotis, 2016; Pagliuso et al., 2016) and control numerous cellular functions such as cytokinesis, ciliogenesis, vesicular trafficking, cell polarity, and lipid droplet formation (Fung et al., 2014; Oh and Bi, 2011; Song et al., 2016; Balla, 2013; Gassama-Diagne and Payrastre, 2009; Gassama-Diagne et al., 2006; Akil et al., 2016; Schink et al., 2016).

The morphology and positioning of intracellular organelles such as the Golgi and ER are critical for the proper transport and delivery of vesicles to maintain cell polarity, tissue homeostasis, and functions

[1]INSERM, Unité 1193, Villejuif 94800, France

[2]Université Paris-Sud, UMR-S 1193, Villejuif 94800, France

[3]Laboratoire de Physique de l'Ecole Normale Supérieure, ENS, Université PSL, CNRS, Sorbonne Université, Université Paris-Diderot, Sorbonne Paris Cité, Paris, France

[4]Instituto de Física de São Carlos, Universidade de São Paulo, São Carlos, Brazil

[5]Institute for Integrative Biology of the Cell (I2BC), CEA, CNRS, Université Paris-Sud, Université Paris-Saclay, 91198 Gif Sur Yvette Cedex, France

[6]Commissariat à l'Energie Atomique et aux Energies Alternatives, 91191 Gif-Sur-Yvette Cedex, France

[7]Institute Curie, PSL Research University, CNRS UMR 144, Paris, France

[8]These authors contributed equally

[9]Lead Contact

*Correspondence: thiam@ens.fr (A.R.T.), ama.gassama@inserm.fr (A.G.-D.)

https://doi.org/10.1016/j.isci.2019.02.015

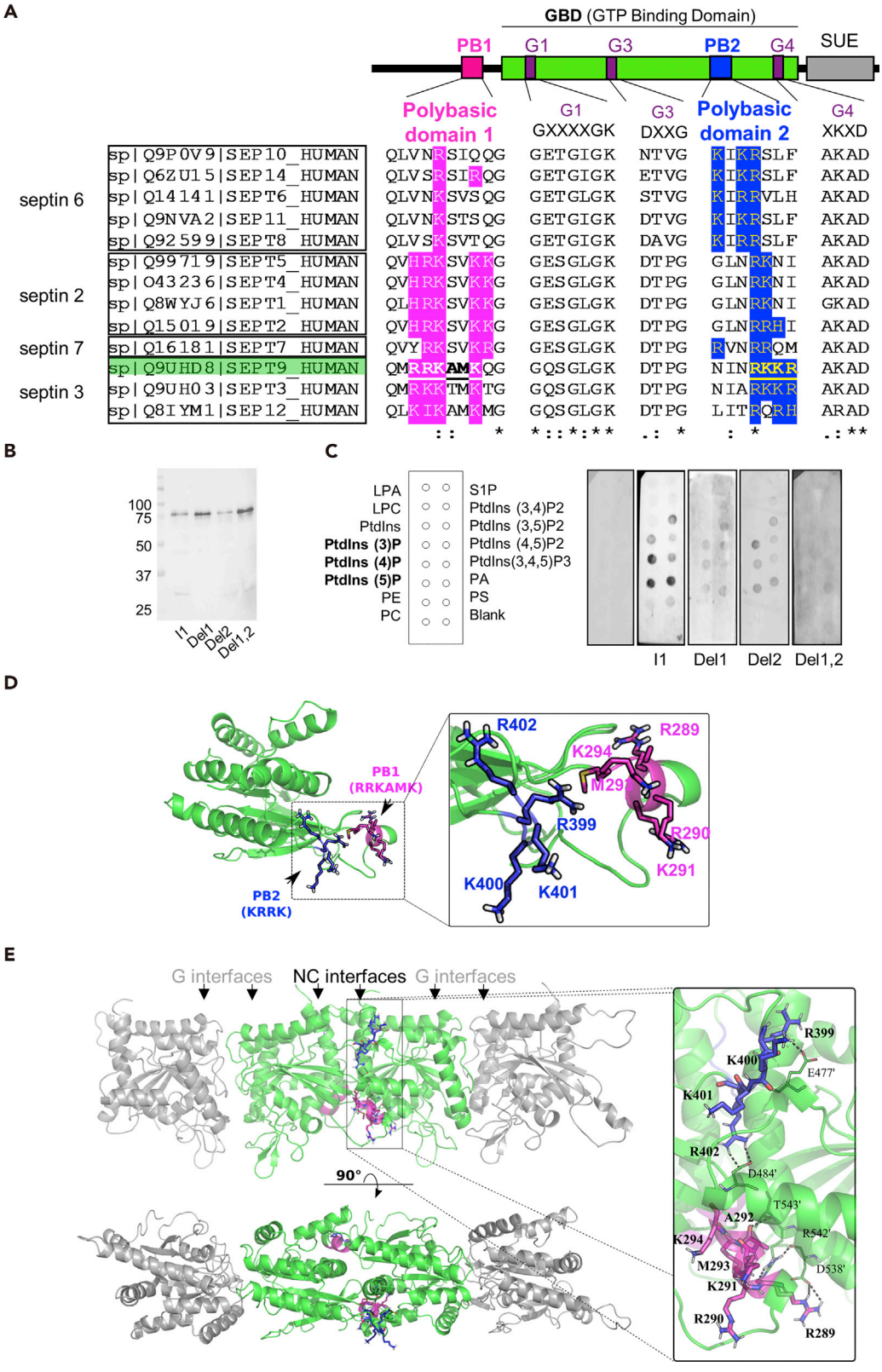
A
GBD (GTP Binding Domain)
PB1
G1
G3
PB2
G4
SUE
Polybasic domain 1
G1 GXXXXGK
G3 DXXG
Polybasic domain 2
G4 XKXD
septin 6
septin 2
septin 7
septin 3
sp|Q9P0V9|SEPT10_HUMAN QLVNRSIQQG GETGIGK NTVG KIKRSLF AKAD
sp|Q6ZU15|SEPT14_HUMAN QLVSRSIRQG GETGIGK ETVG KIKRSLF AKAD
sp|Q14141|SEPT6_HUMAN QLVNKSVSQG GETGLGK STVG KIRRVLH AKAD
sp|Q9NVA2|SEPT11_HUMAN QLVNKSTSQG GETGIGK DTVG KIKRSLF AKAD
sp|Q92599|SEPT8_HUMAN QLVSKSVTQG GETGIGK DAVG KIRRSLF AKAD
sp|Q99719|SEPT5_HUMAN QVHRKSVKKG GESGLGK DTPG GLNRKNI AKAD
sp|O43236|SEPT4_HUMAN QVHRKSVKKG GESGLGK DTPG GLNRKNI AKAD
sp|Q8WYJ6|SEPT1_HUMAN QLHRKSVKKG GESGLGK DTPG GLNRKNI GKAD
sp|Q15019|SEPT2_HUMAN QVHRKSVKKG GESGLGK DTPG GLNRRHI AKAD
sp|Q16181|SEPT7_HUMAN QVYRKSVKRG GESGLGK DTPG RVNRRQM AKAD
sp|Q9UHD8|SEPT9_HUMAN QMRRKAMKQG GQSGLGK DTPG NINRKKR AKAD
sp|Q9UH03|SEPT3_HUMAN QMRKKTMKTG GQSGLGK DTPG NIARKKR AKAD
sp|Q8IYM1|SEPT12_HUMAN QLKIKAMKMG GQSGLGK DTPG LITRQRH ARAD
B
100
75
50
37
25
I1
Del1
Del2
Del1,2
C
LPA
LPC
PtdIns
PtdIns (3)P
PtdIns (4)P
PtdIns (5)P
PE
PC
S1P
PtdIns (3,4)P2
PtdIns (3,5)P2
PtdIns (4,5)P2
PtdIns(3,4,5)P3
PA
PS
Blank
I1
Del1
Del2
Del1,2
D
PB1 (RRKAMK)
PB2 (KRRK)
R402
R289
K294
M293
R399
R290
K291
K400
K401
E
G interfaces
NC interfaces
G interfaces
90°
R399
K400
E477'
K401
R402
D484'
T543'
A292
R542'
K294
M293
D538'
K291
R290
R289

Figure 1. Septin 9 and Human Septins Have Two Polybasic Domains

(A) Top: Schematic representation of the organization of septin domains. Bottom: Multiple alignments of human septins: the polybasic domain 1 (PB1) and polybasic domain 2 (PB2) are highlighted in magenta and blue, respectively. Human septin subgroups are shown in boxes.

(B) Western blot of purified septin 9_i1, septin 9_del1, septin 9_del2, and septin 9_del1,2.

(C) PIP strip overlay assay: PIP strips were incubated with either purified septin 9_i1 (I1), septin 9_del1 (Del1), septin 9_del2 (Del2), or septin 9_del1,2 (Del1,2) proteins at 0.5 μg/mL or with the V5 tag peptide as a negative control and analyzed using the anti-V5 antibody. LPA, lysophosphatidic acid; LPC, lysophosphocholine; PtdIns, phosphatidylinositol; PtdIns(3)P; PtdIns(4)P; PtdIns(5)P; PtdIns(3,4)P2; PtdIns(3,5)P2; PtdIns(4,5)P2; PtdIns(3,4,5)P3; PA, phosphatidic acid; PS, phosphatidylserine; PE, phosphatidylethanolamine; PC, phosphatidylcholine; S1P, sphingosine 1-phosphate.

(D) Model of septin 9 based on the crystal structure (PDB code 5cyp) showing PB1 and PB2.

(E) Model of the septin G9NC/NC9G complex using the simulated dimer of septin 9 at the NC interface and based on the symmetry operations of the crystallographic structure (PDB code 5cyp). The two molecules of septin 9 on either side of the NC interface are in green, and their encompassed PB1 and PB2 are presented in magenta and blue, respectively. The rectangle indicates PB1 and PB2 shown at a higher magnification on the right. The residues for PB1 and PB2 are labeled and outlined in black. Dashed black lines indicate the interaction between the PBs and neighboring septin 9 residues.

(Lavieu et al., 2014; de Forges et al., 2012; van Bergeijk et al., 2016). Such morphological arrangements are often ensured by cytoskeletal factors such as microtubules and actins, which are in part recruited by septins (Tanaka-Takiguchi et al., 2009; Fung et al., 2014; Bridges et al., 2016; Mostowy and Cossart, 2012). However, whether septins directly affect organelle morphology and function is poorly understood (Gurel et al., 2014; Weirich et al., 2008).

Here, by using septin 9 crystal structures and simulations of the molecular dynamics (MD) of the septin 9 monomer and dimer, we have identified the existence of a second polybasic domain (PB2). The deletion of PB2 phenocopied PB1 deletion by reducing the binding capacity of septin 9 to PI lipids and impairing the formation of septin filamented structures, hereinafter referred to simply as filaments. However, *in vitro* flotation assays revealed that the PB domains are not required for septin 9 membrane binding but proffer specificity to PI-containing membranes. These findings prompted us to identify amphipathic helices that are adjacent to the PB domains and possibly mediate the physical association of septin 9 with membranes. We studied the importance of the PB domains on organelles and determined their critical role in Golgi assembly and functionality.

RESULTS

Septins Have a Second Polybasic Domain PB2 that Forms with PB1 a Basic Cluster at the NC Interface

Septins bind to PI lipids via a polybasic domain (PB1) located at the N terminus of their GTP-binding domain (Zhang et al., 1999; Pan et al., 2007). However, we recently found that the deletion of PB1 in septin 9 reduces, but does not abolish, the interaction between septin 9 and monophosphorylated PIs (Akil et al., 2016). This observation prompted us to look for the presence of additional PI-interacting domains. We aligned the sequences of septin 9 and other human septins and identified a second motif enriched in basic amino acids (aa 399–402 of human septin 9 isoform 1; 586 residues) (Figure 1A). This second polybasic domain, which we termed PB2, contains a variable number of basic amino acids (2–4), but is conserved in all human septins (Figure 1A).

We next generated and purified a PB2-deleted mutant (septin 9_del2), a PB1-deleted mutant (septin 9_del1) (Akil et al., 2016), and a mutant lacking both PB1 and PB2 (septin 9_del1,2) (Figure S1A). These proteins displayed band profiles similar to septin 9_i1 (Figures 1B and S1B), which was in a monomeric form based on migration on a native gel (Figure S1C). We then used a phosphatidylinositol phosphate (PIP) strip overlay assay to determine the affinity of septin 9_i1 and its mutant forms with different phospholipid head groups. As expected, we found a specific interaction between septin 9_i1 and phosphatidylinositol (PtdIns) monophosphate (Figure 1C). The interaction signal with PIs was decreased in septin 9_del1 and septin_del2 and was almost abolished in septin 9_del1,2 (Figure 1C). This result supports the idea that both PB domains can mediate the interaction of septin 9 with PIs.

To study the involvement of PB2 in the structural organization of septin 9, we opted for an MD simulation approach using the most resolved septin 9 crystal structure (aa 293–564), PDB code 5cyp. In this structure, the missing residues and side chains were added and completed by amino acids from 276 to 292 (see Methods), which included those of PB1. Regardless of the initially folded state of these added residues, we found one single final equilibrium conformation of the protein where the N-terminal region was pre-folded into an α-helix around PB1 (Figures 1D and S1D). This equilibrated monomer was then

superimposed on the crystal structure of septin 9 (PDB: 5cyp) to build a tetramer that contains the NC-NC interface (Figure 1E). At this interface, PB2 and PB1 appeared to make numerous salt bridges between septin monomers (Figure 1E, black dots in the inset); we found optimal distances between amino acids of the PB domains and those of the adjacent septin. These interactions involved the R399 and R402 residues of PB2 interacting, respectively, with E477′ and D484′, and the R289 residue of PB1 interacting with D538′. The main chain atoms of R289 and A292 in PB1 made hydrogen bonds with R542′ and T543′ of the neighboring septin (Figure 1E). This structural analysis indicates that the PB2 domain forms an extended basic cluster with PB1 at the NC interface of septin 9.

Contribution of PB Domains to Septin 9 Membrane Association

To determine whether the PB domains are equally involved in septin 9 membrane interactions, we first performed MD simulations of the interaction between the monomeric structure of the protein shown in Figure 1D and membranes devoid of PtdIns(4)P (Figure S2A). The simulations were made by leaving the protein close to a dioleoylphosphatidylcholine (DOPC) membrane, thus offering it the opportunity to change conformation over time. We simulated three conditions by changing the initial protein conformation and velocity (Figure S2A, MD1-3). In all cases, septin 9 was recruited to the membrane. However, we found that PB1 was always in contact with the membrane (Figure S2A) (see Transparent Methods), whereas PB2 was not under one of the conditions (Figure S2A, MD1). This observation suggests that PB1 may be better positioned to interact with membranes.

To further clarify the involvement of PB1 and PB2 in septin 9 interactions with PI lipids, we took advantage of the recently resolved crystal structure of septin 3 (Macedo et al., 2013), which belongs to the same subgroup as septin 9 (Figure 1A). By using homology modeling, we built a septin 9 monomer and tetramer (Figures S2B and S2C), and used the tetramer to determine its spatial organization on a DOPC/DOPE bilayer containing PtdIns3P, PtdIns4P and PtdIns(5)P (Lomize et al., 2012). In the membrane-proximal PB1-PB2 cluster of the tetramer, we found that the basic residues R^{289}, R^{290}, K^{291}, and K^{400} were particularly well positioned to interact with the phosphate head group of the PIs (Figure 2A). Three of these residues, namely, R289, R290, and K291, belong to PB1, and K400 to PB2. This analysis also supports the idea that PB1 is more closely involved in regulating septin 9 membrane binding than PB2, which was consistent with the previous MD results (Figure S2A).

Septin 9 Interactions with Membranes *In Vitro* Do Not Require Any of the PB Domains

We decided to study the contribution of PB domains to septin association *in vitro*. Large and small liposomes (e.g., above 300 nm and below 200 nm), containing PtdIns(4)P or not, were, respectively, generated by vortex and high-power sonication, so as to mimic flat and curved membranes. The liposomes were then mixed with septin 9_i1 and septin 9_del1,2. A sucrose gradient flotation assay was subsequently performed (Figure 2B), during which only bound proteins would float up with the liposomes to the top fraction (Figure 2B). The supernatant fraction was collected and the amount of bound proteins determined by western blot (Figure 2C).

As expected, septin_i1 bound more strongly to liposomes containing PtdIns(4)P than to those that lacked PtdIns4P (Figures 2C–2F). However, binding was reduced on smaller liposomes (Figures 2C–2F and S2D), which suggests that the binding capacity of septin 9 was better with flat rather than positively curved membrane regions. Surprisingly, we found that septin 9_del1,2, which lacked both PB domains, bound efficiently to all membranes (Figures 2C–2F), despite the fact that it also had a slight preference for flatter membranes (Figure S2D). This efficient binding of septin 9_del1,2 was not detected in the PIP strip overlay assay because perfect membrane bilayers are not generated using this method (Figure 1C); it was, however, consistent with the binding of septin 9 to membranes devoid of PI lipids obtained by MD simulations (Figure S2A). Finally, the binding of septin 9_del1 and septin 9_del2 was not enhanced by the presence of PtdIns(4)P, and it was almost lost on small liposomes (Figure S2E). These results suggest that PB1 and PB2 are both required for the specific and efficient binding of septin 9 to PI-containing membranes.

In conclusion, our data described above, and particularly those obtained with septin 9_del1,2, suggest that septin 9 can bind bilayer membranes without involving its PB domains. Both PB domains seem to be necessary to provide septin 9 binding selectivity to PI-containing membranes, and especially to flat membranes or at least to those that are not positively curved.

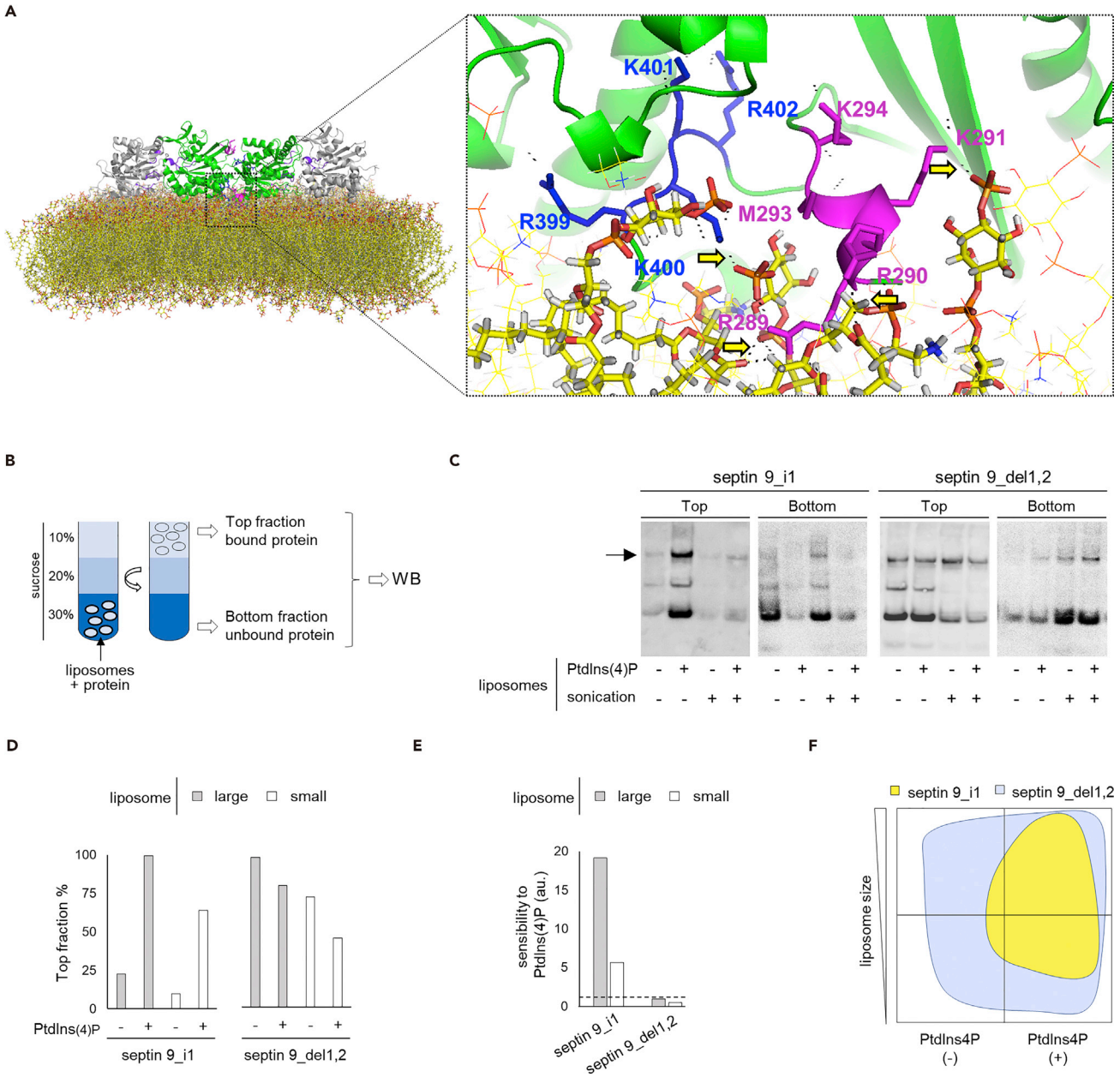

Figure 2. PBs Are Required for Specific Interactions between Septin 9_i1 and PIs and the Recognition of Membrane Forms

(A) Modeling of the septin 9 complex interaction with a patch of PI-containing lipid bilayer. The dotted rectangle indicates the PB1-PB2 area proximal to the membrane shown in higher magnification. The residues for PB1 and PB2 are labeled. Yellow arrows indicate the interaction between PBs and the membrane.

(B) Schematic representation illustrating the liposome floatation assay.

(C) Western blots of septin 9_i1 (I1) and septin 9_del1.2 (Del1,2) subjected to a liposome flotation assay; the arrow indicates the band corresponding to V5-tagged Septin9_i1 (68 kDa), which was further analyzed.

(D) Bar graph representing the percentage of protein in the top fraction (bound protein) from an analysis of the blots presented in (B).

(E) Bar graph representing the sensitivity of the protein to PtdIns(4)P (the ratio of protein bound with PtdIns(4)P(+) liposomes to protein bound with PtdIns(4)P(−) liposomes). Dashed line indicates the 1 value.

(F) Schematic phase diagram illustrating the results of western blot analysis of the liposome flotation assay.

Septins Have PB-Adjacent Amphipathic α-Helix

We next tried to determine how septin 9 was able to interact directly with membranes in the absence of PI lipids and without its PB domains (Figure 2). Many soluble proteins bind membranes using amphipathic

alpha-helix (AH) motifs, which are, moreover, able to detect subtle differences in membrane curvature and charges (Bigay and Antonny, 2012), as is the case for septin 9. We therefore performed a bioinformatics screening for AHs in the full sequence of septin 9. Two striking sequences emerged from our analysis as being the most prominent AHs (aa 274 to 294 and aa 370 to 402). Surprisingly, these AHs were directly adjacent to PB1 and PB2, respectively (Figure 3A). The sequence close to PB1 corresponded to a flexible strand that can fold into an AH, which is probably why it is missing from the septin 9 crystal structure. MD simulation showed that this portion of the protein indeed folded as an α-helix (Figure S1D) and was well positioned to bind membranes (Figure 3A). The AH close to PB2 was folded but oriented toward the interior of the protein, unless a conformational switch occurred. These AHs contain very hydrophobic residues, such as tyrosine, tryptophan, and phenylalanine, a feature that enhances membrane association. Our analysis therefore suggested that septin 9 has at least one PB-adjacent AH associated with PB1 that can mediate its physical association with membranes. In other septins, we also found flagrant AHs juxtaposed with the PB2 of septins 2, 6, and 7 with which septin 9 interacts to form the octamer. We took advantage of the existence of a crystal structure of the trimer formed by septins 2, 6, and 7 to verify the orientation of the AHs. We found that the AH-PB2 of septin 6 was suitably oriented to bind membranes (Figure 3B). The AH feature at the PB1 domain of these septin 9 counterparts was less pronounced (Figures 3B and S3A–S3D).

Septin 9 PB Domains Are Essential for the Formation of Septin Filaments

Our data supported the idea that the AHs of septin 9 are probably the membrane binding motifs that are restricted to PI-containing membranes by the PB domains. Under this scenario, the PB domains would be more available to participate in the NC/NC interactions that mediate the formation of septin higher-order structures.

We transfected HeLa cells with septin 9_i1, which we found was incorporated in higher-order filamentous structures that also contained endogenous septin 9 and septin 2 (Figures 4A and 4B). However, the strong expression of septin 9_i1 seemed to displace endogenous septin 9 from the filaments, whereas septin 2 remained recruited at a similar level (Figures 4B and 4C). Our overexpressed septin 9 construct thus had a dominant negative effect on endogenous septin 9 (Figure S4E). When cells were transfected with the PB-deleted constructs (Del1, Del2, Del1,2), the filamentous structures were lost (Figures 4D–4F) despite the presence of endogenous septin 9. Here also, these constructs displayed the dominant-negative effect of septin 9 (Figure S4E), and septin 2 was not present in the filaments (Figure 4D). These results suggest that both PB domains are involved in septin 9 assembly, in line with our previous results from the structural analysis (Figures 1E and S2C).

To avoid possible conformational changes to the protein and its dysfunction because of the deletion of PB domains, we performed simple point mutations. We substituted the basic lysine and arginine amino acids (K and R) with glutamine (Q), which is a non-charged but polar amino acid that has a long side chain as in K and R; this substitution was therefore optimal to minimize possible conformational changes in the protein. For example, in septin 9_Q1, the R and K residues of PB1 were not deleted as in septin 9_del1, but replaced by Q. We observed that cells transfected with septin 9_Q1, septin 9_Q2, or septin 9_Q1,2 were unable to form septin filaments (Figures S4A–S4C), in the same way as with the deletion (Figures 4D–4F). We next performed simple mutations by substituting one or two R with alanine (A) within PB1, and the filaments were lost once again (Figure S4D). None of these constructs affected the normal expression of endogenous septin 9 (Figure S4E).

In conclusion, the point mutant phenocopied the deletion constructs, and the results suggest that the positively charged PB cluster at the NC/NC interface is essential to the formation of septin filaments.

Septin 9 PB Domains Are Critical for Golgi Assembly

Septin 9 binds mainly to PtdIns(3)P, PtdIns(4)P, and PtdIns(5)P, which are primarily detected in early endosomes (EE), the Golgi apparatus, and the ER, respectively (Pendaries et al., 2006; Kutateladze, 2010; Sarkes and Rameh, 2010). We thus wanted to probe whether PB1 and PB2 contribute to the organization of these endomembrane compartments. We expressed septin 9_i1 and the mutant constructs in HeLa cells and then studied the morphology of these organelles.

A significant increase in EE and ER markers was observed in the perinuclear region of septin 9_i1-expressing cells when compared with empty vector (EV) and septin 9 mutants, which were similar (Figures S5A–S5E).

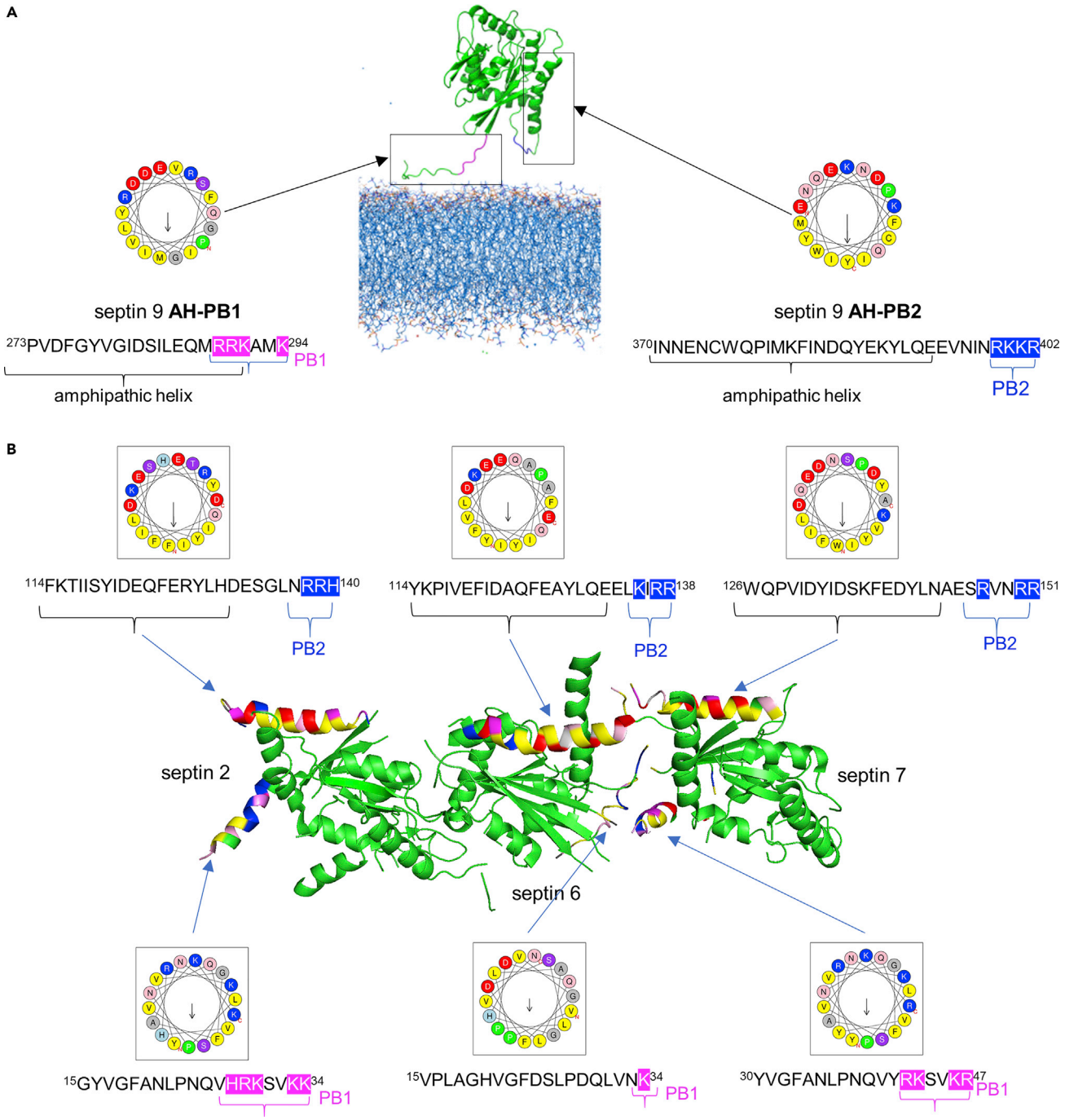

Figure 3. Septin 9 Has Putative PB-Associated Amphipathic Helices Mediating Its Binding to the Membrane

(A) Crystal structural model of septin 9 (PDB code 5cyp) showing the predicted amphipathic helices opposed to PB1 and PB2 and their helical wheel representation generated using Heliquest.

(B) Structural model of the (NC2G/G6NC/NC7G) septin complex published by Sirajuddin et al. showing the predicted amphipathic helices opposed to PB2 and the helical wheel representation of these helices generated using Heliquest. The sequence of each predicted helix is presented; the corresponding helical wheel and PB1 basic residues are highlighted in magenta and those of PB2 in blue.

The most striking observation of the deletion of PB domains was on the Golgi structure (Figures 5A and 5B). In cells expressing septin 9_i1, we found the normal phenotype of a compact Golgi embedded in higher-order structures of septin 9_i1 filaments (Figures 5A and 5C), which contained septins 2, 6, and

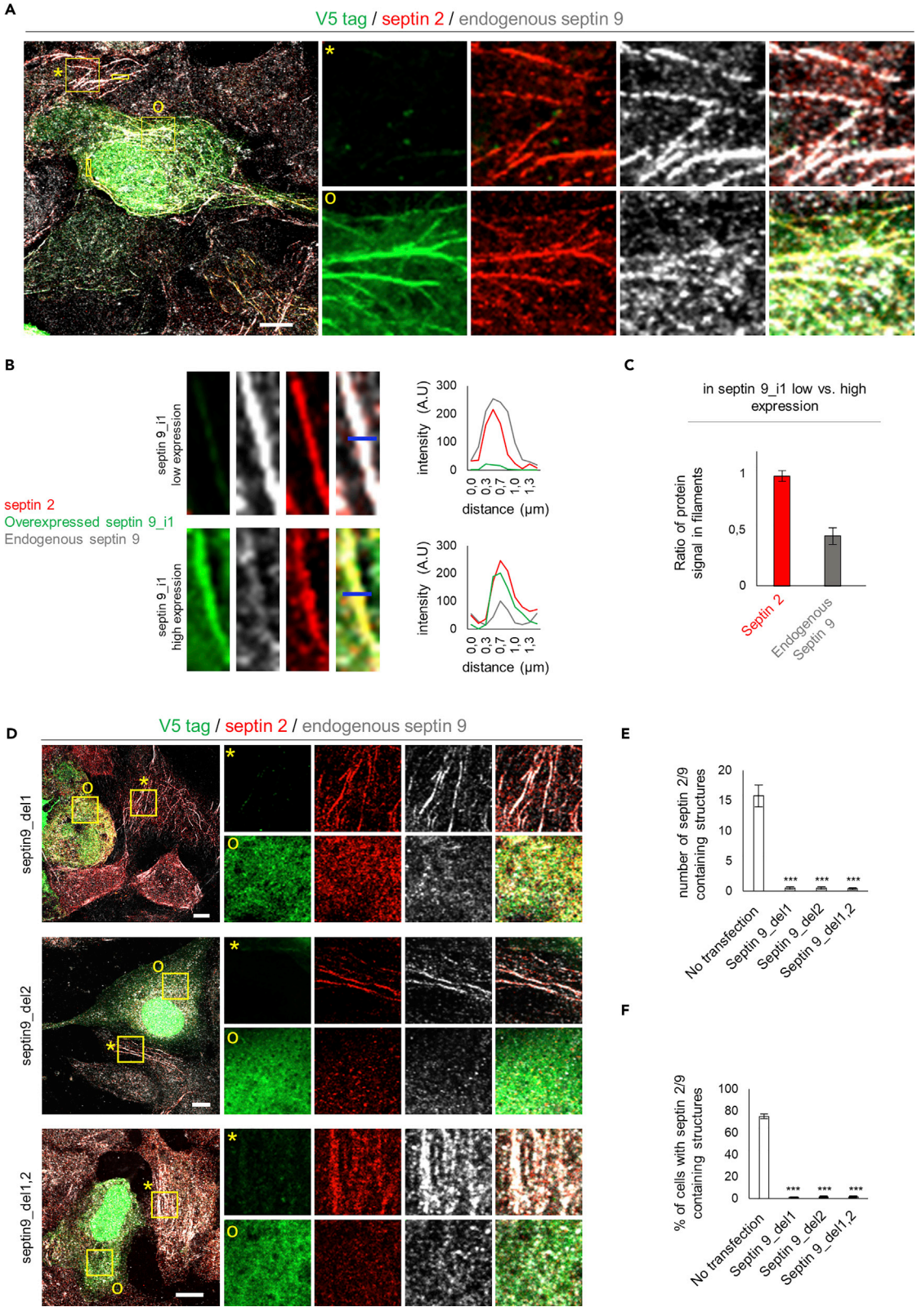
A
V5 tag / septin 2 / endogenous septin 9
B
septin 2
Overexpressed septin 9_i1
Endogenous septin 9
septin 9_i1 low expression
septin 9_i1 high expression
intensity (A.U)
distance (µm)
C
in septin 9_i1 low vs. high expression
Ratio of protein signal in filaments
Septin 2
Endogenous Septin 9
D
V5 tag / septin 2 / endogenous septin 9
septin9_del1
septin9_del2
septin9_del1,2
E
number of septin 2/9 containing structures
No transfection
Septin 9_del1
Septin 9_del2
Septin 9_del1,2
F
% of cells with septin 2/9 containing structures

Figure 4. Overexpressed Septin 9_i1 Replaces Indigenous Septin 9 in Septin Filaments, Whereas PB-Mutated Septin 9 Expression Impairs Them

(A) Huh7,5 cells transfected with septin9_i1 for 48 h and then fixed and stained for V5 tag in green (septin 9_i1), endogenous septin 2 (red) and endogenous septin 9 (gray). * indicates low septin9_i1-expressing cells and O indicates high septin9_i1-expressing cells. Squares indicate the area shown at higher magnification on the right. Scale bar, 10 μm.

(B) Higher-magnification images of the small yellow rectangles shown in (A). On the right, the line graphs show the line profile analysis of the lines shown in these images.

(C) Bar graph showing the ratio of the intensity of endogenous septin 2 and endogenous septin 9 in low septin 9_i1-expressing cells to those of high-septin 9_i1-expressing cells. Values are mean ± SEM from 10 filaments under each condition from two independent experiments.

(D) Huh7,5 cells transfected with septin 9_del1 (Del1), septin 9_del2 (Del2), or septin 9_del1,2 (Del1,2) for 48 h and then fixed and stained for V5 tag (green), endogenous septin 2 (red), and endogenous septin 9 (gray). * indicates a low-expressing or non-transfected cell, and O indicates a transfected cell. Squares indicate the area shown at higher magnification to the right.

(E) Bar graph representing the number of the filament structures containing both endogenous septin 9 and septin 2. Values are mean ± SEM from 10 cells under each condition from two independent experiments *** $P<0.0001$, (Student's t-test).

(F) Bar graph representing the percentage of cells containing filament structures of endogenous septin 9 and septin 2. Values are mean ± SEM from 50 cells under each condition from two independent experiments *** in indicates $P<0.0001$, (Student's t-test).

7 (Figure S5F). Strikingly, the deletion or mutation of any of the PB domains led to Golgi fragmentation (Figures 5A, 5B, and S5G).

Assembly of the Golgi apparatus is dependent on microtubule polymerization (Miller et al., 2009). The depolymerization of microtubules, typically under nocodazole treatment, results in Golgi fragmentation; removal of the nocodazole enables the re-polymerization of microtubules and Golgi reassembly. We thus took MDCK cells stably expressing septin 9_i1 and septin 9_del1,2 and treated them with nocodazole to induce Golgi fragmentation. The nocodazole was then washed out and Golgi reassembly monitored (Figure 5D). In septin 9_i1 cells, the scattered Golgi elements reassembled normally within 20 min (Figures 5D and 5E), but they did not in septin 9_del1,2 cells (Figures 5D and 5E), even after much longer periods of time (Figure S5H).

The aforementioned observations suggest a function for septin filaments in Golgi assembly that is dependent on septin 9 PB domains.

Mutations of PB Domains Cause Golgi Fragmentation, but Not Septin 9 Dissociation from the Membrane

Our data suggested that a lack of PB domains might cause a loss of the specific binding of septin 9 to PtdIns(4)P (Figure 2). We decided to monitor the interaction between septin 9 and PtdIns(4)P within cells. HeLa cells were therefore transfected with the cDNAs of EV, septin 9_i1, and Del1, Del2, or Del1,2 and stained for V5 tag, TGN46 (Golgi marker), and PtdIns(4)P (Figures 6A and S6A).

PtdIns(4)P was strongly co-localized with compact Golgi in EV and septin 9_i1, as had been expected (Dippold et al., 2009). In cells transfected with the Del1, Del2, or Del1,2 constructs (Figure 6A), the Golgi was fragmented, as seen previously, but no significant difference in co-localization between TGN and PtdIns(4)P was noted (Figure 6B). However, we observed a non-significant decrease in the co-localization of septin 9 with PtdIns(4)P (Figure 6C) that varied between the different transfected constructs. PB-deleted mutants still displayed strong signals on small spherical compartments, which were possibly Golgi ministacks, vesicles, or other structures (Figures 6A and S6A). To determine whether the mutant septin 9 proteins were associated with these membrane structures, we permeabilized the cells and removed the soluble proteins before fixation. We observed that the septin 9 mutated protein signal remained on intracellular structures (Figure 6D). This observation suggests that a lack of PB domains does not prevent the binding of mutant proteins to possible membrane structures, in line with our *in vitro* assays that revealed the ability of the mutants to bind to membranes (Figure 2). To further test this finding, a subcellular fractionation assay was performed (Figure S6B) and showed that septin 9_i1 always peaked with the Golgi marker, whereas septin 9_del1,2 had a more spread out signal, suggesting that it probably bound to other membranes, including fragmented Golgi elements (Figure S6B).

Taken together, our results suggest that PB1 and PB2 restrict septin 9 binding to PI-containing membranes, such as PtdIns(4)P on Golgi, but are not directly responsible for septin membrane association. They play a major function in septin complex assembly and subsequent organelle structuration.

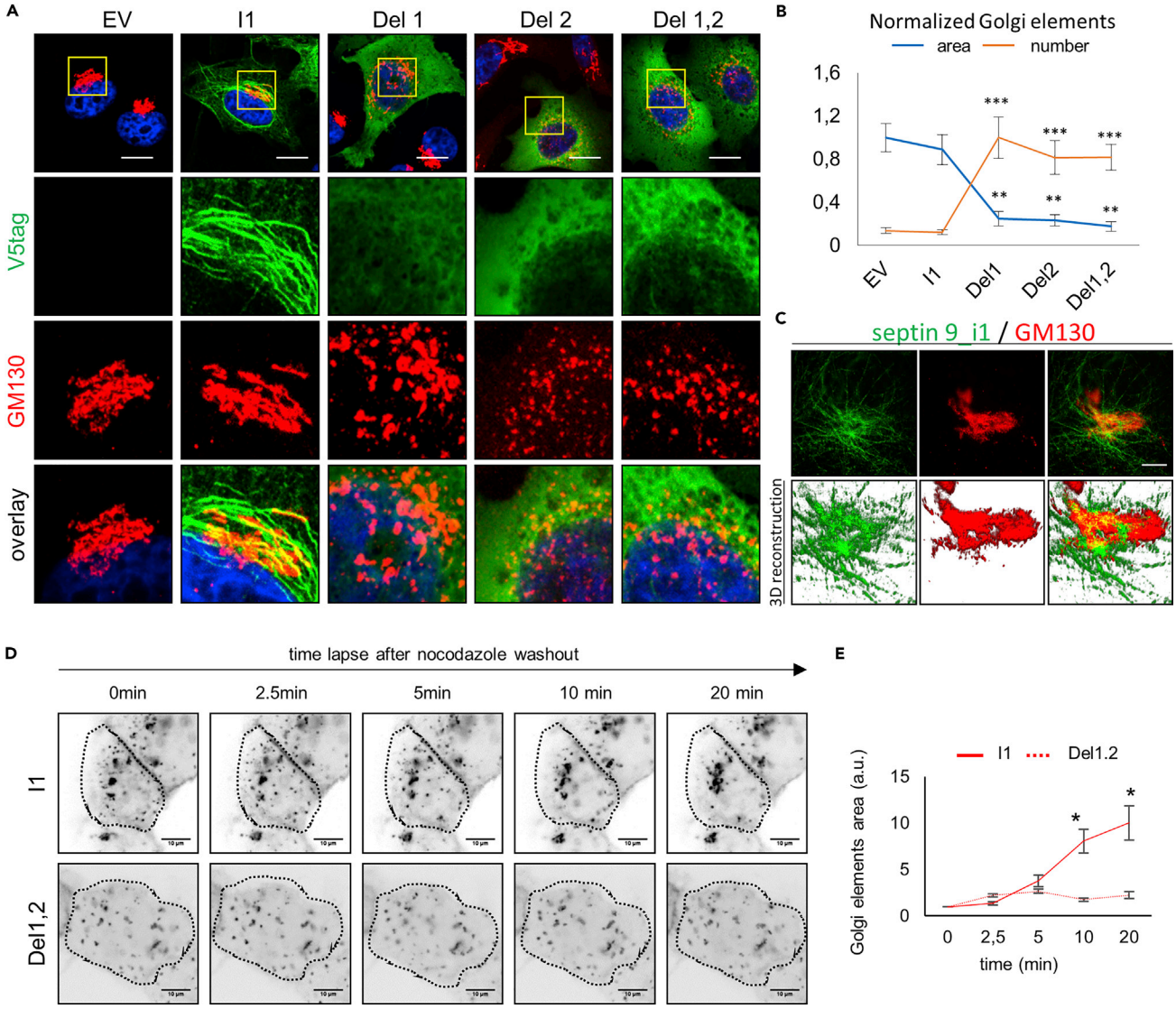

Figure 5. Septin 9 Localizes to Golgi and Is Required to Ensure Its Compact Morphology

(A) HeLa cells transfected with an empty vector (EV), septin 9_i1 (I1), septin 9_del1 (Del1), septin 9_del2 (Del2), or septin 9_del1,2 (Del1,2) for 48 h and then fixed and stained for Golgi with GM130 (red) and V5tag (green). Squares indicate the area shown at higher magnification below. Scale bar, 10 μm.

(B) Line graph representing the normalized number and size of Golgi elements. Values are mean ± SEM from 15 cells under each condition for three independent experiments. **$p < 0.001$, ***$p < 0.0001$ (Student's t test).

(C) Stimulated emission depletion microscopy (STED) high-resolution microscopic images of HeLa cells transfected with septin9_i1 (I1) and then fixed and stained for GM130 (red) and V5tag (green). Images are shown in 3D reconstructions below. Scale bar, 5 μm.

(D) MDCK cells stably expressing septin 9_i1 or septin 9_del1,2, transfected with KDE-GFP for 24 h, and subjected to nocodazole washout. Images represent video frames illustrating the reassembly of Golgi after the removal of nocodazole.

(E) Dotted lines indicate the cell periphery. Line graphs to the right represent fold increases in Golgi elements relative to time 0 during three experiments. Scale bar, 10 μm. *$p < 0.05$ (Student's t test).

Endogenous Septin 9 Localizes to Golgi and Regulates Its Compactness and Functionality

The transfection of our septin 9 mutant constructs, which had a dominant-negative effect on endogenous septin 9, could be the reason for Golgi fragmentation. We therefore studied this endogenous septin 9 and found that it also co-localized with Golgi (Figure 7A). This observation was likewise supported by a subcellular fractionation assay (Figure 7B) in which both septin 2 and septin 9 peaked with GM130 (Figure 7B). These results suggest that endogenous septin 9 is present in septin structures associated with the Golgi apparatus.

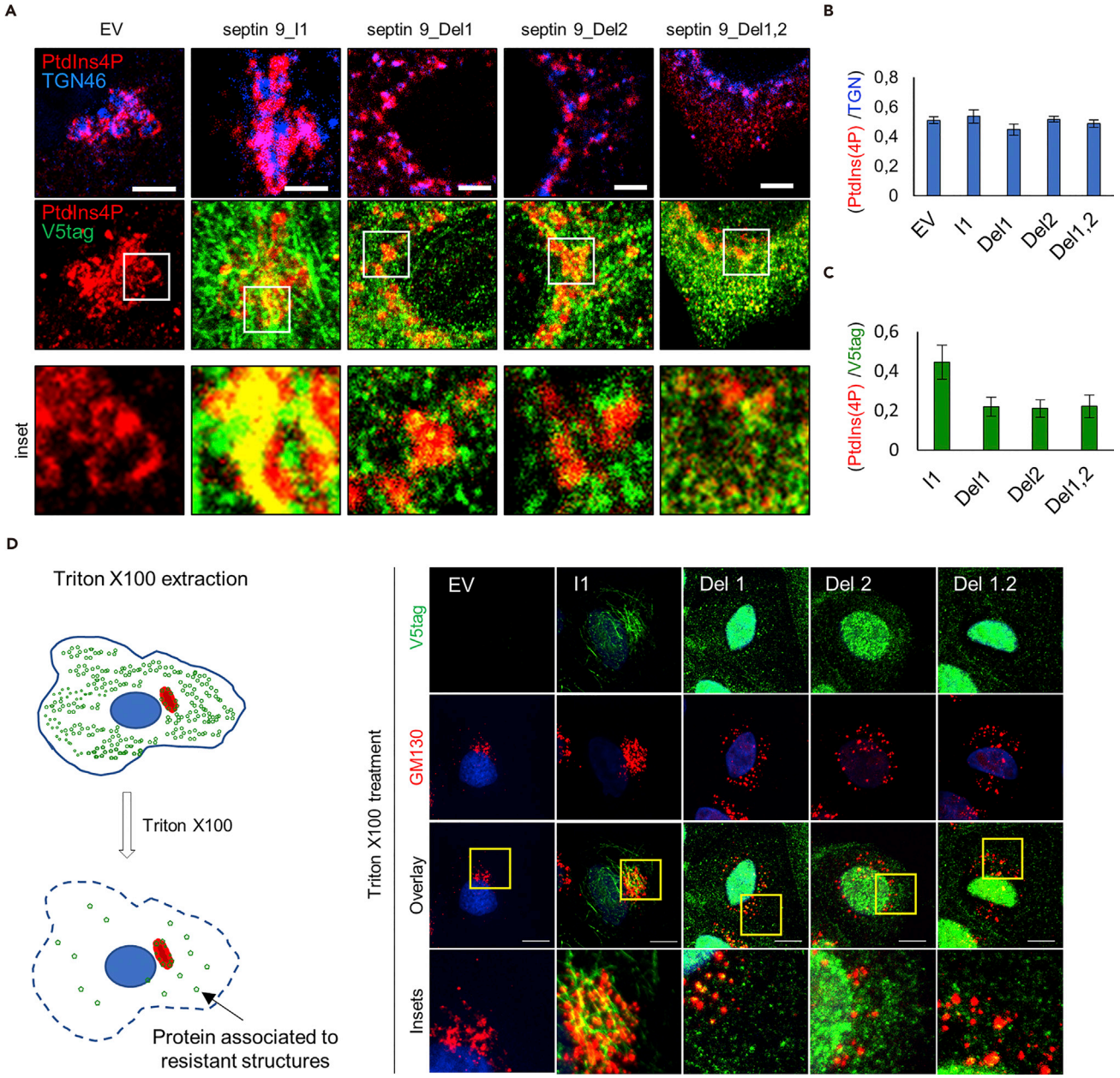

Figure 6. PBs Are Required for the Specific Recruitment of Septin 9_i1 to the Golgi

(A) HeLa cells were transfected with an empty vector (EV), septin 9_i1 (I1), septin 9_del1 (Del1), septin 9_del2 (Del2), or septin 9_del1,2 (Del1,2) for 48 h before being fixed and stained for PtdIns(4)P (red), TGN46 (blue), and V5tag (green). Squares indicate the area shown below at higher magnification. Scale bar, 3 μm.

(B) Bar graph represents Pearson's correlation coefficient (Rr) analysis of PtdIns(4)P and TGN46. Values are mean ± SEM of 10 cells under each condition from three experiments.

(C) Bar graph representing Pearson's correlation coefficient (Rr) analysis of PtdIns(4)P and V5 tag. Values are mean ± SEM of 10 cells under each condition from three experiments.

(D) Left, schematic representation illustrating cell extraction with Triton X-100. On the right, MDCK stably transfected with EV, septin 9_i1 (I1), septin_9 del1 (Del1), septin_9 del2 (Del2), or septin_9 del1.2 (Del1,2) were grown for 24 h on coverslips. The cells were then extracted using cold PBS buffer containing Triton X-100 at 0.1% for 30 s and then fixed and stained for V5tag (green) and GM130 (red). Scale bar, 10 μm.

We next worked with a cell line stably transfected with septin 9 small interfering RNA (siRNA) (Figure 7C). In control cells, giantin, which is also a Golgi marker, displayed polarized and compact features, i.e., enriched on one side of the nucleus (Figure 7C). However, in the septin 9 siRNA cells, we observed a fragmentation of the Golgi (Figure 7C). Interestingly, this fragmentation could be rescued by transfection with septin 9_i1

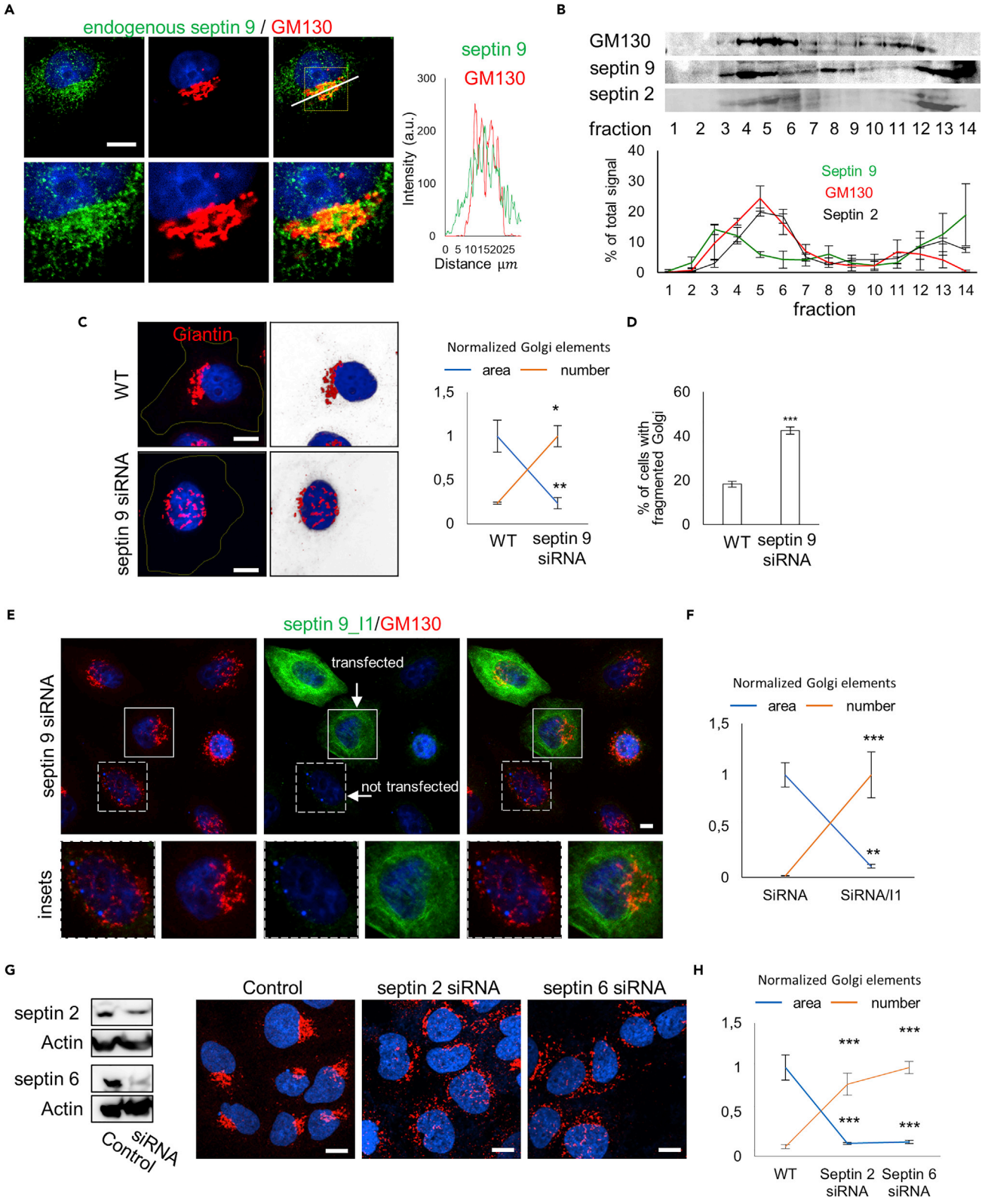
A
endogenous septin 9 / GM130
septin 9
GM130
Intensity (a.u.)
Distance μm
B
GM130
septin 9
septin 2
fraction 1 2 3 4 5 6 7 8 9 10 11 12 13 14
% of total signal
Septin 9
GM130
Septin 2
fraction
C
Giantin
WT
septin 9 siRNA
Normalized Golgi elements
area
number
WT
septin 9 siRNA
D
% of cells with fragmented Golgi
WT
septin 9 siRNA
E
septin 9_I1/GM130
septin 9 siRNA
transfected
not transfected
insets
F
Normalized Golgi elements
area
number
SiRNA
SiRNA/I1
G
septin 2
Actin
septin 6
Actin
siRNA
Control
Control
septin 2 siRNA
septin 6 siRNA
H
Normalized Golgi elements
area
number
WT
Septin 2 siRNA
Septin 6 siRNA

Figure 7. Septin 9 Localizes to Golgi and in the Same Way as Septins Is Required to Ensure Its Compact Morphology

(A) Huh7 cells fixed and stained for septin 9 and GM130. Scale bar, 5 μm. On the right, line profile of the white line shown in the merge image.

(B) Huh7 cells were grown for 48 h before being subjected to a subcellular fractionation assay and analyzed with western blot for septin 9 and GM130 and septin 2. The line graph below shows densitometry analysis of the subcellular fractionation assay. Values are mean ± SEM from three independent experiments.

(C) Septin 9 siRNA and control cells stained for giantin (red). Cells are shown in 2D images with a black background and in 3D reconstruction images with a white background. Scale bar, 10 μm. The right line graph represents the normalized size and number of Golgi elements. Values are mean ± SEM of 150 cells from three independent experiments. *$p < 0.05$, **$p < 0.001$ (Student's t test).

(D) Percentage of cells with fragmented Golgi obtained from three independent experiments. At least 800 cells were counted for each condition. Values are mean ± SEM. ***$p < 0.0001$ (Student's t test).

(E) Septin 9 siRNA cells were transfected with septin 9_i1 and stained for GM130 (red) V5tag (green). Squares indicate the area shown at higher magnification below. Scale bar, 10 μm.

(F) Bar graph representing the size and number of Golgi elements in 20 cells from two independent experiments performed as described in (E). **$p < 0.001$, ***$p < 0.0001$ (Student's t test).

(G) Huh7.5 cells transfected with septin 2 siRNA or septin 6 siRNA for 48 h were analyzed with western blot (left) and confocal microscopy for GM130 (red) (right). Scale bar, 10 μm.

(H) Line graph representing the normalized size and number of Golgi elements in 10 cells from two independent experiments. ***$p < 0.0001$ (Student's t test).

(Figures 7E and 7F), but not with the PB-deleted constructs (Figures S7A and S7B). Here again, we performed the nocodazole washout assay, which confirmed that Golgi reassembly is dependent on endogenous septin 9 (Figure S7C), which therefore plays an important role in maintaining the compact structure of the Golgi.

Our overall data suggest that septin 9 (endogenous and septin 9_i1) is incorporated into filaments that are critical to the Golgi structure. As septin 2 and septin 6 are involved in these filaments, they should also control Golgi compactness. We accordingly found that their depletion by a specific siRNA promoted Golgi fragmentation (Figures 7G, 7H, and S7E). These data reinforced our model in which septin complexes are incorporated into the filament structures that are associated with the Golgi membrane and control its compactness.

Finally, fragmentation of the Golgi apparatus is known to impede secretory pathways (Xiang et al., 2013; Lavieu et al., 2014; Joshi et al., 2015). We thus probed whether septin 9 depletion (Figures S8A and S8B) impeded these pathways. We first used a Venus-tagged neuropeptide Y construct (NPY-Venus) as a model of secreted protein; we determined its level of secretion in the cell culture medium and lysates. We found that septin 9 depletion resulted in a significant decrease of secreted NPY-Venus (Figure S8C). We next studied the trafficking of a temperature-sensitive variant of the vesicular stomatitis virus G protein tagged with GFP (tsVSVG-GFP) (this protein remains in the ER at 40°C but enters the secretory pathway when the temperature is lowered to 32°C; Presley et al., 1997). Control and septin 9-depleted cells were transfected with tsVSVG-GFP and fixed at different time points after the temperature was lowered from 40°C to 32°C (Figure S8D). After 2 h, the protein signal in the Golgi area was greatly reduced in control cells, whereas it remained intact in septin 9-depleted cells, suggesting a defect in intracellular trafficking. Taken together, these data indicate that septin 9 plays a critical role in Golgi compactness and its subsequent function in cellular trafficking.

DISCUSSION

Septins belong to the family of GTPase proteins that assemble into macrostructure filaments, which are important to the membrane-remodeling processes. Here we have shown that septin 9 is particularly necessary for Golgi structure and function, as the absence of septin 9 provokes Golgi dissociation and impairs secretory pathways. Our results support the idea that septin 9 and other septins (such as septin 2 and septin 6) form a filament matrix that harbors Golgi stacks.

The association of septins with membranes was previously thought to be specifically mediated by an interaction between their polybasic domain PB1 and PI lipids (Pan et al., 2007; Zhang et al., 1999; Tanaka-Takiguchi et al., 2009; Casamayor and Snyder, 2003). Here we found that septin membrane association was much more subtly regulated. First, we identified the presence of a second polybasic domain (PB2) in septin 9, which is conserved among the different human septins and regulates the interaction between septin and PI lipids. Second, we identified AH structures adjacent to PB1 and PB2, which probably mediate the physical association of septin 9 with membranes. Our results support the idea that PB1 and PB2 may act

together to restrict the binding of these AHs of septin 9 to PI-containing membranes, and particularly to non-positively curved membranes. This conclusion is in line with the *in vivo* accumulation of septins in specific plasma membrane ingressions or concavities, such as cleavage furrows (Spiliotis and Nelson, 2006). Finally, based on our *in vitro* observations, MD (Figure S2A), and modeling of the interaction between the septin 9 complex and PtdIns(4)P-containing membranes (Figure 2A), PB1 appears to be more closely involved in regulating septin 9 membrane-binding specificity than PB2, but both are critical for septin filament assembly.

Whether septin 9 acts in a cellular context in the monomeric form is not known. Apart from the septin 9 isoform septin 9_i4, which has been found in non-filament structures (Chacko et al., 2005), most septins have been so far been reported as being incorporated in filamentous structures, and whether they exist under monomeric form is also unknown. Despite our *in vitro* studies having been performed with the monomeric septin 9, our results provided information on how septin 9 membrane-binding determinants might influence the localization of septin oligomers to membranes. These results are consistent with a recent report on the presence of AH structures in oligomeric septin filaments, capable of sensing macroscopic curvatures (Cannon et al., 2019).

Based on our results, we propose that septin 9 binds membranes with AHs that can strongly associate to the membrane. In this setting, PB domains may interact with PI lipids to dock the protein on specific organelles, thereby preventing non-specific binding. This mechanism would enrich the protein on the membrane thanks to the PBs, and stabilize it through the action of AHs.

It is not yet clear how septins control the Golgi structure. One hypothesis is that the PB domains contribute to enriching septin 9 or octameric complexes in Golgi elements. Assembly of the octamers would form the septin filaments, which will in the meantime have brought different Golgi elements close enough to promote their fusion, e.g., by SNARE proteins. Under this hypothesis, a septin matrix will form a structure embedding the Golgi elements. This model is consistent with our experiments on Golgi reassembly after nocodazole treatment: this reassembly occurred with septin 9_i1, whereas with Del1,2 (Figures 5D, 5E, S5H) or septin 9 depletion (Figure S7C) it did not. Consistent also with our model, the Golgi is fragmented by the depletion of septin 2 or 6. Hence our study has revealed the importance of higher-order septin structures in Golgi homeostasis. As microtubules and actin filaments are also known to maintain Golgi structure and interact with septins (Miller et al., 2009; Egea et al., 2006; Kondylis et al., 2007; Fung et al., 2014), it is plausible that septins are engaged in hybrid filaments with microtubules and actin to maintain Golgi structure.

On other organelles, we observed that PB1 and PB2 affected ER and EE organization, which was reminiscent of the role that we described for septin 9 in lipid droplet dynamics; interestingly, septin filaments have been seen to be prominent around large lipid droplets (Akil et al., 2016). This particular localization of septin higher-order structures to sites of micron-scale membrane curvature is emerging as an important feature of organelle dynamics (Cannon et al., 2019).

Finally, septin structures have been proposed to act as a physical barrier against the non-specific docking of vesicles on the active zone of the synapse (Yang et al., 2010). Thus septin structures may also behave as physical barriers that prevent the collapse of Golgi stacks or their connection to other organelles. Our findings on the role of septin 9 in the Golgi apparatus could probably be extended to other organelles and offer a paradigm for the structural and biological functions of septins.

Limitation of the Study

One limitation of this study is that the septin 9 protein studied *in vitro* is in monomeric form, whereas it is unknown whether it can exist in such form in cells.

METHODS

All methods can be found in the accompanying Transparent Methods supplemental file.

SUPPLEMENTAL INFORMATION

Supplemental Information can be found online at https://doi.org/10.1016/j.isci.2019.02.015.

ACKNOWLEDGMENTS

This work received support in the form of a grant from the Association pour la Recherche sur le Cancer (ARC/SUBV/CKLQ6) for A.G.D. and from the ANRS (France Recherche Nord & sud SIDA - hiv Hépatites: FRENSH) through a grant to S.B. and a PhD fellowship for C.T. A.R.T is supported by the ANR-TERC (LDEN), Paris Sciences et Lettres, and ATIP-Avenir. We would like to thank H. Russell (Queen's University, Belfast, UK) for providing the septin 9_i1 construct. We also thank A. Baillet (Université Paris-Sud, UMR-S 1193, Villejuif, France) for access to live cell imaging facilities.

AUTHOR CONTRIBUTIONS

A.G.-D., M.O., and A.R.T. designed the research, analyzed the data, and wrote the paper. M.O. conducted the experiments, with the support of C.P, B.G., N.B., D.S., C.T., and A.R.T. C.T. purified the recombinant proteins. A.S.C. and R.C.G. analyzed septin 9 crystal structures and performed the molecular dynamics simulations using these structures. C.T. and S.B. with the help of R.G., J.Y., and T.T. performed the septin 9 homology modeling and septin 9/PIs interaction modeling.

DECLARATION OF INTERESTS

The authors declare no competing interests.

Received: June 1, 2018
Revised: October 12, 2018
Accepted: February 13, 2019
Published: March 29, 2019

REFERENCES

Akil, A., Peng, J., Omrane, M., Gondeau, C., Desterke, C., Marin, M., Tronchère, H., Taveneau, C., Sar, S., Briolotti, P., et al. (2016). Septin 9 induces lipid droplets growth by a phosphatidylinositol-5-phosphate and microtubule-dependent mechanism hijacked by HCV. Nat. Commun. *7*, 12203.

Balla, T. (2013). Phosphoinositides: tiny lipids with giant impact on cell regulation. Physiol. Rev. *93*, 1019–1137.

van Bergeijk, P., Hoogenraad, C.C., and Kapitein, L.C. (2016). Right time, right place: probing the functions of organelle positioning. Trends Cell Biol. *26*, 121–134.

Bigay, J., and Antonny, B. (2012). Curvature, lipid packing, and electrostatics of membrane organelles: defining cellular territories in determining specificity. Dev. Cell *23*, 886–895.

Bridges, A.A., Jentzsch, M.S., Oakes, P.W., Occhipinti, P., and Gladfelter, A.S. (2016). Micron-scale plasma membrane curvature is recognized by the septin cytoskeleton. J. Cell Biol. *213*, 23–32.

Cannon, K.S., Woods, B.L., Crutchley, J.M., and Gladfelter, A.S. (2019). An amphipathic helix enables septins to sense micrometer-scale membrane curvature. J. Cell Biol. https://doi.org/10.1083/jcb.201807211.

Casamayor, A., and Snyder, M. (2003). Molecular dissection of a yeast septin: distinct domains are required for septin interaction, localization, and function. Mol. Cell. Biol. *23*, 2762–2777.

Chacko, A.D., Hyland, P.L., McDade, S.S., Hamilton, P.W., Russell, S.H., and Hall, P.A. (2005). SEPT9_v4 expression induces morphological change, increased motility and disturbed polarity. J. Pathol. *206*, 458–465.

Dippold, H.C., Ng, M.M., Farber-Katz, S.E., Lee, S.-K., Kerr, M.L., Peterman, M.C., Sim, R., Wiharto, P.A., Galbraith, K.A., Madhavarapu, S., et al. (2009). GOLPH3 bridges phosphatidylinositol-4-phosphate and actomyosin to stretch and shape the golgi to promote budding. Cell *139*, 337–351.

Dolat, L., and Spiliotis, E.T. (2016). Septins promote macropinosome maturation and traffic to the lysosome by facilitating membrane fusion. J. Cell Biol. *214*, 517–527.

Egea, G., Lázaro-Diéguez, F., and Vilella, M. (2006). Actin dynamics at the Golgi complex in mammalian cells. Curr. Opin. Cell Biol. *18*, 168–178.

de Forges, H., Bouissou, A., and Perez, F. (2012). Interplay between microtubule dynamics and intracellular organization. Int. J. Biochem. Cell Biol. *44*, 266–274.

Fung, K.Y.Y., Dai, L., and Trimble, W.S. (2014). Cell and molecular biology of septins. Int. Rev. Cell Mol. Biol. *310*, 289–339.

Gassama-Diagne, A., and Payrastre, B. (2009). Phosphoinositide signaling pathways: promising role as builders of epithelial cell polarity. Int. Rev. Cell Mol. Biol. *273*, 313–343.

Gassama-Diagne, A., Yu, W., ter Beest, M., Martin-Belmonte, F., Kierbel, A., Engel, J., and Mostov, K. (2006). Phosphatidylinositol-3,4,5-trisphosphate regulates the formation of the basolateral plasma membrane in epithelial cells. Nat. Cell Biol. *8*, 963–970.

Gurel, P.S., Hatch, A.L., and Higgs, H.N. (2014). Connecting the cytoskeleton to the endoplasmic reticulum and Golgi. Curr. Biol. *24*, R660–R672.

Joshi, G., Bekier, M.E., and Wang, Y. (2015). Golgi fragmentation in Alzheimer's disease. Front. Neurosci. *9*, 340.

Kim, M.S., Froese, C.D., Estey, M.P., and Trimble, W.S. (2011). SEPT9 occupies the terminal positions in septin octamers and mediates polymerization-dependent functions in abscission. J. Cell Biol. *195*, 815–826.

Kondylis, V., van Nispen tot Pannerden, H.E., Herpers, B., Friggi-Grelin, F., and Rabouille, C. (2007). The golgi comprises a paired stack that is separated at G2 by modulation of the actin cytoskeleton through Abi and Scar/WAVE. Dev. Cell *12*, 901–915.

Kutateladze, T.G. (2010). Translation of the phosphoinositide code by PI effectors. Nat. Chem. Biol. *6*, 507–513.

Lavieu, G., Dunlop, M.H., Lerich, A., Zheng, H., Bottanelli, F., and Rothman, J.E. (2014). The Golgi ribbon structure facilitates anterograde transport of large cargoes. Mol. Biol. Cell *25*, 3028–3036.

Lomize, M.A., Pogozheva, I.D., Joo, H., Mosberg, H.I., and Lomize, A.L. (2012). OPM database and PPM web server: resources for positioning of proteins in membranes. Nucleic Acids Res. *40*, D370–D376.

Macedo, J.N.A., Valadares, N.F., Marques, I.A., Ferreira, F.M., Damalio, J.C.P., Pereira, H.M., Garratt, R.C., and Araujo, A.P.U. (2013). The structure and properties of septin 3: a possible missing link in septin filament formation. Biochem. J. *450*, 95–105.

Miller, P.M., Folkmann, A.W., Maia, A.R.R., Efimova, N., Efimov, A., and Kaverina, I. (2009). Golgi-derived CLASP-dependent microtubules control Golgi organization and polarized

trafficking in motile cells. Nat. Cell Biol. *11*, 1069–1080.

Mostowy, S., and Cossart, P. (2012). Septins: the fourth component of the cytoskeleton. Nat. Rev. Mol. Cell Biol. *13*, 183–194.

Nishihama, R., Onishi, M., and Pringle, J.R. (2011). New Insights into the phylogenetic distribution and evolutionary origins of the septins. Biol. Chem. *392*, 681–687.

Oh, Y., and Bi, E. (2011). Septin structure and function in yeast and beyond. Trends Cell Biol. *21*, 141–148.

Pagliuso, A., Tham, T.N., Stevens, J.K., Lagache, T., Persson, R., Salles, A., Olivo-Marin, J.-C., Oddos, S., Spang, A., Cossart, P., et al. (2016). A role for septin 2 in Drp1-mediated mitochondrial fission. EMBO Rep. *17*, 858–873.

Pan, F., Malmberg, R.L., and Momany, M. (2007). Analysis of septins across kingdoms reveals orthology and new motifs. BMC Evol. Biol. *7*, 103.

Pendaries, C., Tronchère, H., Arbibe, L., Mounier, J., Gozani, O., Cantley, L., Fry, M.J., Gaits-Iacovoni, F., Sansonetti, P.J., and Payrastre, B. (2006). PtdIns5P activates the host cell PI3-kinase/Akt pathway during Shigella flexneri infection. EMBO J. *25*, 1024–1034.

Peterson, E., and Petty, E. (2010). Conquering the complex world of human septins: implications for health and disease. Clin. Genet. *77*, 511–524.

Presley, J.F., Cole, N.B., Schroer, T.A., Hirschberg, K., Zaal, K.J., and Lippincott-Schwartz, J. (1997). ER-to-Golgi transport visualized in living cells. Nature *389*, 81–85.

Sarkes, D., and Rameh, L.E. (2010). A novel HPLC-based approach makes possible the spatial characterization of cellular PtdIns5P and other phosphoinositides. Biochem. J. *428*, 375–384.

Schink, K.O., Tan, K.-W., and Stenmark, H. (2016). Phosphoinositides in control of membrane dynamics. Annu. Rev. Cell Dev. Biol. *32*, 143–171.

Sellin, M.E., Sandblad, L., Stenmark, S., and Gullberg, M. (2011). Deciphering the rules governing assembly order of mammalian septin complexes. Mol. Biol. Cell *22*, 3152–3164.

Sirajuddin, M., Farkasovsky, M., Hauer, F., Kühlmann, D., Macara, I.G., Weyand, M., Stark, H., and Wittinghofer, A. (2007). Structural insight into filament formation by mammalian septins. Nature *449*, 311–315.

Song, K., Russo, G., and Krauss, M. (2016). Septins as modulators of endo-lysosomal membrane traffic. Front. Cell Dev. Biol *4*, 124.

Spiliotis, E.T., and Nelson, W.J. (2006). Here come the septins: novel polymers that coordinate intracellular functions and organization. J. Cell Sci. *119*, 4–10.

Tanaka-Takiguchi, Y., Kinoshita, M., and Takiguchi, K. (2009). Septin-mediated uniform bracing of phospholipid membranes. Curr. Biol. *19*, 140–145.

Weirich, C.S., Erzberger, J.P., and Barral, Y. (2008). The septin family of GTPases: architecture and dynamics. Nat. Rev. Mol. Cell Biol. *9*, 478–489.

Xiang, Y., Zhang, X., Nix, D.B., Katoh, T., Aoki, K., Tiemeyer, M., and Wang, Y. (2013). Regulation of protein glycosylation and sorting by the Golgi matrix proteins GRASP55/65. Nat. Commun. *4*, 1659.

Yang, Y.-M., Fedchyshyn, M.J., Grande, G., Aitoubah, J., Tsang, C.W., Xie, H., Ackerley, C.A., Trimble, W.S., and Wang, L.-Y. (2010). Septins regulate developmental switching from microdomain to nanodomain coupling of Ca(2+) influx to neurotransmitter release at a central synapse. Neuron *67*, 100–115.

Zhang, J., Kong, C., Xie, H., McPherson, P.S., Grinstein, S., and Trimble, W.S. (1999). Phosphatidylinositol polyphosphate binding to the mammalian septin H5 is modulated by GTP. Curr. Biol. *9*, 1458–1467.

ISCI, Volume *13*

Supplemental Information

Septin 9 has Two Polybasic Domains Critical to Septin Filament Assembly and Golgi Integrity

Mohyeddine Omrane, Amanda Souza Camara, Cyntia Taveneau, Nassima Benzoubir, Thibault Tubiana, Jinchao Yu, Raphaël Guérois, Didier Samuel, Bruno Goud, Christian Poüs, Stéphane Bressanelli, Richard Charles Garratt, Abdou Rachid Thiam, and Ama Gassama-Diagne

TRANSPARENT METHODS

The molecular dynamics simulations

The monomer of septin 9 (Figure 1C) was built, using Coot program (Emsley et al., 2010). by adding the missing residues from chain A of the crystal structure 5cyo (which has the less number of missing residues of all solved structures for septin 9), completing the sequence from residue 275 to 563. Missing side chains were also added and we made a 1 ns NPT equilibration restraining all main chain atoms but the ones from the added residues (plus direct neighbor residues) slowly increasing the temperature from 0 to 310K. The entire structure was then equilibrated in the same manner prior to the 100 ns MD (Figure S2A).

The dimer of septin 9 (Figure 1E) was built using the above-mentioned conformation of septin 9 monomer after the missing residues were equilibrated, considering only residues from 294 to 563. Two of these conformations were superposed to the crystal structure 5cyp at the NC interface. A pre-folded N-terminal region, comprising residues 275 to 295, was added to each chain in two different orientations: one by superposing the residues 294 and 295 from the two structures and the other by superposition with the PB1 residues of the crystal structure of septin 3 (PDB code 4z54). This pre-folded N-terminal region was obtained after a 500 ns MD simulation (Figure S1D), performed in triplicate (two of them with a amide at the C-terminal), which started from a stretched random conformation of this residues manually built with Coot program (Emsley et al., 2010).

The MDs (Figure S2A) were performed with the Gromacs program (Abraham et al., 2015) using the united-atom force field gromos54a7 (Schmid et al., 2011) and a leap-frog algorithm for integrating Newton's equations of motion. Explicit solvation was used with SPC/E water model (Berendsen HJC et al.) and the DOPC membrane coordinates were obtained from the Gromacs website and the topology from Peter Tieleman's group (Tieleman et al., 2000). Periodic boundary conditions were used through all the simulations, with the long-range electrostatic interactions treated by particle mesh Ewald method (Darden et al.). The short-range non-bonded interactions were amputated with 10 Å cutoff. Bond lengths involving H atoms were constrained using the Linear Constraint Solver (LINCS) algorithm (Hess et al.). The temperature was controlled by Nosé-Hoover thermostat (Cheng and Merz, 1996), while the pressure coupling was maintained isotropic in the axes parallel to the membrane plane and different in the normal direction with the Parrinello-Rahman barostat (Parrinello and Rahman, 1981). For each simulation (MD1, MD2 and MD3) (Figure S2A) the average of contacts with the membrane atoms that appeared during these simulations were counted and are shown as bar

graphs: MD1 and MD3 have the same starting protein conformation but MD1 has a lower protein velocity; MD2 has a different starting protein conformation than MD1 and MD3 but has the same initial velocity as MD3. We considered a contact whenever a protein atom was less than 4Å from a lipid atom –non-hydrogen atoms only. In MD1, the average was calculated for the entire period of 100 ns, and the conformations were sampled each 10 ps.

Homology modeling

Rebuilding the structure of septin 3 (59-350)

The crystal model of septin 3 comprises residues 59-350 of human neuronal-specific septin 3 in a complex with GDP (Macedo et al., 2013). The ordered part of this construct harbors 75% sequence identity with residues 297-565 of human septin 9 (isoform_i1; 586 residues). It starts immediately after PB1 (^{289}RRKAMK^{294}) and contains PB2 (^{399}RKKR^{402}).

We carefully completed and rebuilt the septin 3 GTPase domain G dimer available (PDB code 3SOP) using Coot (Emsley et al., 2010) and phenix.refine (Adams et al., 2010). As well as correcting a few local errors, we were able to reliably model all the missing loops, except for the N-terminus of switch I (corresponding to septin 9 residues 323-333), and most of the missing sidechains. Sidechains for which no density was apparent were still included in the most likely rotamer, given the chemical environment. The final structure comprised the counterparts of septin 9 residues 297-565 (less residues 323-333) and was refined to R_work = 0.2039, R_free = 0.2612, from the initial values of R_work = 0.2585, R_free = 0.2780.

Homology modeling using the Rosetta of septin 9 297-565 4-molecule filament

A septin 3, 4-molecule filament with a single NC interface was generated by means of crystallographic symmetry. The filament model of septin 9 297-565 was built using Rosetta 3.5 (Das and Baker, 2008) according to the following steps: 1) the RosettaCM comparative modelling pipeline (Song et al., 2013) was used to build a monomeric septin 9 model (Figure S2B), taking a septin 3 monomer (residues 59-350) as the template; 2) the Rosetta relax protocol

was used first of all to refine the NC interface under C2 symmetry constraints, while regions distant from the NC interface remained fixed; 3) the G interface was refined in a similar way under C2 symmetry constraints, without moving the NC interface. In particular, a dozen distance constraints were carefully introduced into this step to preserve the nucleotide binding site as in the GDP-bound state; 4) finally, GDP and Mg were copied into the monomeric model and the filament was built by symmetry (Figure S2C).

Modeling of PB1 in the context of septin 9 4-molecule filament and membrane orientation

The threading server I-Tasser (Yang et al., 2015) was used to add septin 9 residues 288-296 (including PB1) to the 297-565 Rosetta model. Although two orientations of PB1 are possible in the context of a septin 9 monomer, only a conformation pointing away from the NC interface is consistent with filament formation across this interface (Figure S2B). We introduced this conformation into the septin 9 tetrameric model (Figure S2C). The orientation of this filament relative to a membrane was then computed using the energy transfer method implemented in the PPM server (Lomize et al., 2012).

PC-PE-PIP /septin 9 membrane generation and optimization

The position predicted by the PPM server was used as input to the CHARMM-GUI (Wu et al., 2014) in order to add a 200x200 $Å^2$ lipid bilayer to the septin 9 tetramer. The lipid composition was chosen to be identical for both leaflets: 55% POPC, 25% POPE, 10% POPI5P, 5% POPI3P and 5% POPI4P. This protein-membrane system was energy-minimized, equilibrated and subjected to a 10-ns molecular dynamic simulation using GROMACS (Berendsen et al., 1995) and the CHARMM36 force field update for lipids. We used the GROMACS protocols encoded in the scripts generated by CHARMM-GUI to perform this simulation (Lee et al., 2016) (Figure 2A).

Cell lines and culture conditions

septin 9 HeLa SilenciX (septin 9 siRNA and control cell lines) was purchased from TiboLab. HeLa and huh7 cells were maintained in a DMEM complete media composed of Dulbecco's modified Eagle's Medium (DMEM; Invitrogen) containing 4.5 g/l glucose and supplemented with 10% heat-inactivated fetal bovine serum, 1% non-essential amino acids (GibcoBRL) and 1% penicillin/streptomycin (GibcoBRL). septin 9 siRNA and control cell lines were maintained in a DMEM complete media supplemented with hygromycin B (Invitrogen)100 µg/ml. MDCK cells were maintained in MEM complete medium composed of Minimum Essential Media (MEM; Invitrogen) supplemented with 5% heat-inactivated fetal bovine serum and 1% penicillin/streptomycin (GibcoBRL). MDCK stably transfected cells of septin 9_i1 and mutant protein were maintained in MEM complete medium supplemented with G418 (Invitrogen) at 400 µg/ml.

Plasmids

The cDNA of the septin 9 isoform 1 transcript within the pcDNA3.1/V5-His-TOPO vector (septin 9_i1) or within the pET21d vector (pET21d septin 9_i1), PB1-deleted septin 9 within the pcDNA3.1/V5-His-TOPO vector (septin9_del1), and the pET21d vector (pET21d septin 9_del1), as previously described (Akil et al., 2016), were used during this study. Septin 9_del2 (PB2-deleted septin 9) and septin 9_del1.2 (PB1and PB2 deleted septin 9), pcDNA septin 9_Q1 (R and K residues were substituted with Q in PB1) , pcDNA septin 9_Q2 (R and K residues were substituted with Q in PB2) pcDNA septin 9_Q1.2 (R and K residues were substituted with Q in PB1and PB2), pcDNA septin 9_R289A (R289 of PB1 was substituted with A), pcDNA septin 9_R289/290A (R289 and R290 of PB1 was substituted with A) were generated using the QuikChange II XL Site-Directed Mutagenesis Kit (Cat#200521) from Agilent, in

accordance with the manufacturer's recommendations.

Septin 9_del2 V5/His tag and septin 9_del1.2 V5/His sequences were thus amplified by PCR from their corresponding pcDNA3.1/V5-His-TOPO vectors. The resulting DNA fragments were inserted in a pET21d vector using the In-Fusion HD Cloning kit Cat#639648 pET21d (Clontech), according to the manufacturer's recommendations, in order to obtain pET21d septin 9_del2 V5/His and PET21d septin 9_del1.2 V5/His. All the primer sequences are presented in Supplementary Table 1.

KDE-GFP (Dipeptidyl peptidase IV in which the extracellular domain had been replaced by the GFP sequence to restrict protein localization to the Golgi apparatus, which we used to visualize this apparatus during live cell imaging experiments) was a gift from Professor Christian Poüs (Paris-Sud University, France). NPY-Venus and tsVSVG-GFP were a gift from Professor Bruno Goud, Institut Curie, PSL Research University. Septin 6 (h) siRNA Cat#sc40938, septin 2 (h) siRNA Cat#40937 were from santacruz biotechnology.

Chemicals:

PIP strip Cat#P-6001, PtdIns4P diC8 Cat#P4008 were purchased from Echelon; Nocodazole Cat#487928 from Calbiochem, and Albumin BSA FFA Cat#126575 came from Calbiochem (1,2-oleoyl-sn-glycero-3-phosphocholine (DOPC) (Cat#850375 Avanti).

Antibodies

Anti-septin 9 Cat#ab38314 (WB:1/500, IF:1/25), anti-septin 2 Cat#ab88657(WB:1/500, IF:1/50), anti-septin 6 Cat#ab138036 (WB:1/500, IF:1/50), Anti α-tubulin Cat#ab15246 (IF:1/100), anti-giantin Cat#ab37266 (IF:1/100), mouse and rabbit anti-V5 tag Cat#ab27671 (WB:1/1,000, IF:1/400), Cat#ab9116 (WB:1/1,000, IF:1/400), FITC conjugated Cat#ab1274 (IF: 1/400) , anti-EEA1 Cat#ab2900 (IF:1/100) and anti-calreticulin Cat#ab2907 (IF:1/100) were obtained from Abcam; anti βtubulin Cat# T4026 (IF:1/100) came from Sigma-Aldrich;

anti-Actin Cat#sc-1616 (WB:1/1,000), anti-GM130 Cat# 610822 were sourced from BD Transduction Laboratories, anti-PtdIns(4)P Cat#Z-P004 (IF:1/100) was obtained from Echelon Biosciences, and anti-TGN46 Cat#NB110-62093 from Novus.

Secondary antibodies: Anti-mouse IgG-HRP and anti-rabbit IgG-HRP came from GE Healthcare (WB:1/1,000). Anti-goat IgG-HRP Cat#sc-2020 (WB: 1/1,000) came from Santa Cruz. Alexa Fluor 633 Cat#A21136, A21070 and A21082 (IF: 1/100), Alexa Fluor 568 Cat#A11004, A11011, A11057 and A21099 (IF:1/100), Alexa Fluor 488 Cat#A11001, A21206 and A21202 (IF:1/100), and nuclei stained with Hoechst Cat#H21486 (IF:1/5,000) were purchased from Life Technology.

Immunofluorescence staining:

Cells were grown on coverslips, fixed with 4% paraformaldehyde for 20 min. and permeabilized for 20 min. at 37°C using a permeabilizing buffer (PFS): DPBS containing saponin (Cat#10294440 Fisher Scientific) 0.025% m.v^{-1} and gelatin from cold water fish skin (Cat#G7041 Sigma 0.7% m.v^{-1}). The cells were then incubated with primary antibody for 2 h and washed three times for 5 min. with PFS before being incubated with the appropriate secondary antibodies or with the dye for 90 min. The coverslips were mounted using Prolong Gold (Cat#P36934, Invitrogen).

Image acquisition and analysis

Images acquired with a Leica TCS SP5 AOBS tandem confocal microscope were analyzed using the Icy bioimage analysis software for 3D reconstruction. For co-localization analysis, images were treated with ImageJ software, and the 'Intensity Correlation Analysis' plug-in was used to generate Pearson's correlation coefficient (Rr) values which ranged from −1 (perfect exclusion) to +1 (perfect correlation).

To determine the distributions of EEA1 and calreticulin in cells, the ‘Radial profile’ plug-in was used. For analysis, a circle was defined at the periphery of each cell and the plug-in produced a profile plot of normalized integrated intensities around concentric circles as a function of distance from a point in the image, considered here as the center of the cell. The concentric circles were assembled in three circle bands, the first corresponding to the area of the nuclei and the rest corresponding to the cytoplasm which was divided in two equal bands (the band near the nucleus being considered as ‘perinuclear’ and the other as the ‘periphery’). The intensity in each band was calculated from the total integrated intensities around the concentric circles present in the band.

To calculate the size and number of Golgi elements, images obtained by confocal microscopy were processed by background subtraction and standardized thresholding (default). The cell ROI was obtained using a freehand selection tool, and then the size and number of Golgi elements were determined by ImageJ particle analysis function (particle areas smaller than 0.01 μm2 were excluded).

The Golgi compactness index, which determines a dimensionless circularity of Golgi elements, was computed according to the formula 4 (sum (areas)/(sum(perimeters))∧2). The values of this index ranged from 1 (perfect compactness) to 0 (perfect fragmentation)(Bard et al., 2003).

For endogenous septin 9 analysis in the filaments of high and low septin 9_i1 expressed cells (Figure 4 panel B and C) we have calculated the ratio of septin 9 intensity in a filament of septin 9_i1 low expression to that of high expression. To ensure that we compare a similar filament in size we have calculated the ratio of septin 9 in a filament with similar septin 2 intensity for that we have the ratio of septin 2 at a value of almost 1 and we observed how the septin 9 ratio will vary.

Liposome floatation assay:

Liposomes were prepared as follows. Two quantities of 1.5µM of DOPC were dissolved in chloroform and dried to a film under nitrogen gas. 1ml of HKM buffer (50 mM Hepes, 120 mM K acetate, and 1 mM MgCl2, pH 7,4.) was added to the first quantity and vortexed to produce the control liposomes (PtdIns4P (-)). The same volume of HKM buffer containing PtdIns4P at 50µM was added to the second quantity and vortexed to produce phospoinositide 4 monophosphate containing liposomes (PtdIns4P (+)) at 3.33% (PtdIns4P to DOPC molar percentage). All the liposomes thus produced were then subjected to seven freeze–thaw cycles and considered as large liposomes. 500µl of PtdIns4P(-) and PtdIns4P(+) large liposomes were then sonicated for 30 seconds to generate the small liposomes.

septin 9-i1 and mutant proteins were added to 200 µl of liposome to a final concentration of 0,1µM, were mixed with an equal volume of sucrose at 75% and then layered on the bottom of a 1-ml thick wall ultracentrifugation tube. 200µl of 20% sucrose and 200 µl of 10% sucrose and 200 µl of HKM buffer were then layered successively. Each tube was subjected to centrifugation at 30,000 rpm using a SW60 rotor (Beckman) for one hour at 4°C. The liposomes were collected from the top 100 µl of the gradient (top fraction) and 100 µl were collected from the bottom of the tub (bottom fraction). The collected fractions were then analyzed using Western blot. The sum of the three bands detected by the V5 antibody in each lane was used to generate the presented results in Figure 2 and Figure S2. To analyze the sensitivity of the protein to bind the PtdIns4P we have calculated the ratio of detected protein in the top fraction of PtdIns4P(+) to that of PtdIns4P(-) in the case of big liposomes and small liposomes and we have call it protein sensitivity to PtdIns4P. To analyze the sensitivity of the protein to bind the small liposomes we have calculated the ratio of detected protein in the top fraction of the small liposomes to that bound to big liposomes in the case of PtdIns4P(+) liposomes and PtdIns4P(-) liposomes and we have call it protein sensitivity to curvature.

Subcellular fractionation assay

Confluent monolayers of cells were placed on ice, washed twice with ice-cold PBS at pH 7.4, and then 10 mM Tris/HCl (pH 7.4) buffer was added for 1min. The cells were scraped into a homogenization buffer comprising 10 mM Tris/HCl, 1 mM EGTA, 0.5 mM EDTA and 0.25 M sucrose, at pH 7.4, which also contained Complete^{TM} protease inhibitors. The result was homogenized with ten strokes of a loose-fitting Dounce homogenizer. All subsequent steps were carried out at 4°C. Post-nuclear supernatants (PNS) were obtained by centrifugation for 10 min at 1000 g. PNS (2 ml) were layered onto a sucrose gradient [successive layers of 1 ml of sucrose at 40% (w/v), 1 ml at 30%, 2ml at 25%, 2ml at 20%, 2ml at 15% and 2 ml at 10%]. The gradients were centrifuged for at least 16 h at 175,000 rpm. After centrifugation, twelve 1-ml fractions were harvested, starting at the top of the gradient. The pellet was re-suspended in 1 ml 0.25 M sucrose (Waugh et al., 2003) (Figure S6B). In Figure 7B, thirteen fractions were collected and the pellet was designated as fraction 14.

Protein production and purification

Escherichia coli BL21(DE3) Rosetta cells were transformed using pET21d septin 9_i1 V5/His, PET21d septin 9_del1 V5/His, PET21d septin 9_del2 and PET21d septin 9_del1,2 V5/His V5/His vectors, and were all incubated with a culture medium containing 100 µg/mL ampicillin and 34 µg/mL chloramphenicol. Cells from a single colony were used to seed an overnight 20 ml pre-culture of LB medium. 1 L LB medium cultures from these pre-cultures were grown at 37°C under agitation to reach an optical density ($OD_{600\ nm}$) of 0.9. The temperature was lowered to 28°C and protein expression was then induced with 1mM Isopropyl β-D-1-thiogalactopyranoside (IPTG) from Sigma, for 4 hours. The cells were harvested by centrifugation and the pellet was stored at -80°C until use. The cell pellet was suspended in 15 mL of 50 mM sodium phosphate at pH 7.4, 300 mM sodium chloride, 10% glycerol, 20 mM imidazole, 0.1% Triton X-100 and one protease inhibitor cocktail EDTA-free tablet (Roche).

Cell lysis was performed by sonication on ice and the cell lysate was clarified by centrifugation for 30 min. at 4°C and 40,000 rpm. After filtering the supernatant, the protein was isolated on a 1 mL metal affinity column (HisTrap HP, GE Healthcare) pre-equilibrated in 50 mM sodium phosphate pH 7.4, 300 mM sodium chloride, 10% glycerol, 20 mM imidazole and then eluted with 50 mM sodium phosphate pH 7.4, 300 mM sodium chloride and 300 mM Imidazole. The fractions containing the protein of interest were further purified by cation exchange chromatography. The pooled fractions were diluted at a ratio of 1:5 to obtain a final solution of 30 mM Tris pH8, 100 mM NaCl, 1 mM EDTA and then incubated with 1 mL of a strong cation exchange resin (Macro-Prep 25S, BioRad). The resin was packed in a column and eluted using a 100 to 600 mM NaCl linear gradient. Fractions containing a majority of protein were obtained at around 350 mM NaCl. The proteins were then flash-frozen and stored at -80°C.

Determination of helix properties

Helical wheels were generated using the Heliquest server (Gautier et al., 2008) **http://heliquest.ipmc.cnrs.fr/**

PIP strip overlay assay

PIP Strip membranes (Echelon Biosciences) were blocked with 3% BSA FFA dissolved in phosphate-buffered saline (PBS) containing 0.1% Tween 20 (3% BSA FFA PBS-T) at room temperature for 60 min., then incubated overnight at 4°C with the same buffer containing the purified protein of interest at a concentration of 0.5 μg ml−1, or the purified V5 tag peptide at an equivalent molar concentration, to act as a control. The membranes were then washed, and bound proteins were detected using a suitable antibody.

tsVSVG secretion assay:

Sept9siRNA and control cells were transfected with tsVSVG-GFP and incubated at 37°C for 3h then at 40°C for a further 16h before being incubated at 32°C for the indicated time in the

presence of

50 µg/ml cycloheximide (Cat: C4859 Sigma). After incubation, cells were fixed and stained.

Immunoblotting

The cells were washed with ice-cold DPBS and lysed on ice using the following buffer: 20 mM Tris, HCl, 100 mM NaCl and 1% Triton X100 at PH 7.4 containing protease inhibitors (cOmplete™ ULTRA Cat#05892970001 Roche). The proteins were separated on SDS (sodium dodecyl sulfate) polyacrylamide gel and electro-transferred onto nitrocellulose membranes. After transfer, the membranes were saturated in DPBS containing 0.1% Tween 20 and 5% milk. Primary antibodies were added overnight at 4°C or for 2 h at room temperature, depending on the antibody. The membranes were then washed with DPBS and incubated for 1 h at room temperature with appropriate secondary antibodies coupled with peroxidase. The ECL plus kit (Cat#32132), SuperSignal™ West Femto Maximum Sensitivity Substrate (Cat#34095) from Thermo Scientific were used for protein detection. Chemiluminescent signals were detected by the G:BOX Chemi Fluorescent & Chemiluminescent Imaging System from SYNGENE. The blots were quantified using ImageJ software. For native purified protein separation (Figure S1C). NativePAGE™ 3-12% Bis-Tris Protein Gels, cat# BN1001BOX from Thermo Fisher scientific were used then the protein were electro-transfered onto PVDF membrane then treated as described above. For NPY analysis in culture medium (Figure S8C), 40µl of culture medium were separated by SDS-PAGE and then processed as indicated above.

Nocodazole washout assay

Cells were grown on 12-mm glass coverslips and allowed to attach overnight before being incubated with a culture medium containing nocodazole (2.5µg/ml) for 1 hour at 37°C, then for 2 hours on ice. The cells were rinsed five times on ice using ice-cold medium in order to remove the nocodazole and were then moved to a pre-warmed medium (at 37°C) (time 0) and incubated

at that temperature for the indicated time before being fixed and stained.

To detect microtubules in the washout experiments, soluble tubulin was eliminated first of all in order to reduce background fluorescence. For this purpose, cells were extracted with MT-stabilizing buffer (80 mM Pipes, 1 mM MgCl2, 2 mM EGTA; pH 6.9) containing 0.1% Triton X-100 (37°C, 30 seconds), and then washed twice with Triton-free buffer at room temperature before being fixed with methanol at -20°C(Poüs et al., 1998).

Imaging the assembly of Golgi apparatus after the removal of nocodazole was achieved using an AXIO-OBSERVER Z1 – COLIBRI® – TIRF 3 VIDEOMICROSCOPE with 6 s between frames, and an exposure of 200 ms (inverted images) (Fig. 3b).

Statistical analyses

Unpaired Student's t-tests were performed and statistical significance was determined at *P <0.05, ** P <0.001 and ***P < 0.0001.

Reference

Abraham, M.J., Murtola, T., Schulz, R., Páll, S., Smith, J.C., Hess, B., and Lindahl, E. (2015). GROMACS: High performance molecular simulations through multi-level parallelism from laptops to supercomputers. SoftwareX *1–2*, 19–25.

Adams, P.D., Afonine, P.V., Bunkóczi, G., Chen, V.B., Davis, I.W., Echols, N., Headd, J.J., Hung, L.-W., Kapral, G.J., Grosse-Kunstleve, R.W., et al. (2010). PHENIX: a comprehensive Python-based system for macromolecular structure solution. Acta Crystallogr. D Biol. Crystallogr. *66*, 213–221.

Akil, A., Peng, J., Omrane, M., Gondeau, C., Desterke, C., Marin, M., Tronchère, H., Taveneau, C., Sar, S., Briolotti, P., et al. (2016). Septin 9 induces lipid droplets growth by a phosphatidylinositol-5-phosphate and microtubule-dependent mechanism hijacked by HCV. Nat Commun *7*, 12203.

Bard, F., Mazelin, L., Péchoux-Longin, C., Malhotra, V., and Jurdic, P. (2003). Src Regulates Golgi Structure and KDEL Receptor-dependent Retrograde Transport to the Endoplasmic Reticulum. J. Biol. Chem. *278*, 46601–46606.

Berendsen, H.J.C., van der Spoel, D., and van Drunen, R. (1995). GROMACS: A message-passing parallel molecular dynamics implementation. Computer Physics Communications *91*, 43–56.

Berendsen HJC, Grigera JR, and Straatsma TP The missing term in effective pair potentials -

The Journal of Physical Chemistry (ACS Publications).

Cheng, A., and Merz, K.M. (1996). Application of the Nosé−Hoover Chain Algorithm to the Study of Protein Dynamics. J. Phys. Chem. *100*, 1927–1937.

Darden, T., York, D., and Pedersen, L. Particle mesh Ewald: An N·log(N) method for Ewald sums in large systems: The Journal of Chemical Physics: Vol 98, No 12.

Das, R., and Baker, D. (2008). Macromolecular modeling with rosetta. Annu. Rev. Biochem. *77*, 363–382.

Emsley, P., Lohkamp, B., Scott, W.G., and Cowtan, K. (2010). Features and development of Coot. Acta Crystallogr. D Biol. Crystallogr. *66*, 486–501.

Gautier, R., Douguet, D., Antonny, B., and Drin, G. (2008). HELIQUEST: a web server to screen sequences with specific alpha-helical properties. Bioinformatics *24*, 2101–2102.

Hess, B., Bekker, H., JC Berendsen, H., and Fraaije GEM, J. LINCS: A linear constraint solver for molecular simulations - Hess - 1997 - Journal of Computational Chemistry - Wiley Online Library.

Lee, J., Cheng, X., Swails, J.M., Yeom, M.S., Eastman, P.K., Lemkul, J.A., Wei, S., Buckner, J., Jeong, J.C., Qi, Y., et al. (2016). CHARMM-GUI Input Generator for NAMD, GROMACS, AMBER, OpenMM, and CHARMM/OpenMM Simulations Using the CHARMM36 Additive Force Field. J Chem Theory Comput *12*, 405–413.

Lomize, M.A., Pogozheva, I.D., Joo, H., Mosberg, H.I., and Lomize, A.L. (2012). OPM database and PPM web server: resources for positioning of proteins in membranes. Nucleic Acids Res. *40*, D370-376.

Macedo, J.N.A., Valadares, N.F., Marques, I.A., Ferreira, F.M., Damalio, J.C.P., Pereira, H.M., Garratt, R.C., and Araujo, A.P.U. (2013). The structure and properties of septin 3: a possible missing link in septin filament formation. Biochem. J. *450*, 95–105.

Parrinello, M., and Rahman, A. (1981). Polymorphic transitions in single crystals: A new molecular dynamics method. Journal of Applied Physics *52*, 7182–7190.

Poüs, C., Chabin, K., Drechou, A., Barbot, L., Phung-Koskas, T., Settegrana, C., Bourguet-Kondracki, M.L., Maurice, M., Cassio, D., Guyot, M., et al. (1998). Functional Specialization of Stable and Dynamic Microtubules in Protein Traffic in WIF-B Cells. J Cell Biol *142*, 153–165.

Schmid, N., Eichenberger, A.P., Choutko, A., Riniker, S., Winger, M., Mark, A.E., and van Gunsteren, W.F. (2011). Definition and testing of the GROMOS force-field versions 54A7 and 54B7. Eur. Biophys. J. *40*, 843–856.

Song, Y., DiMaio, F., Wang, R.Y.-R., Kim, D., Miles, C., Brunette, T., Thompson, J., and Baker, D. (2013). High-resolution comparative modeling with RosettaCM. Structure *21*, 1735–1742.

Tieleman, D.P., van der Spoel, D., and Berendsen, H.J.C. (2000). Molecular Dynamics Simulations of Dodecylphosphocholine Micelles at Three Different Aggregate Sizes: Micellar

Structure and Chain Relaxation. J. Phys. Chem. B *104*, 6380–6388.

Waugh, M.G., Minogue, S., Anderson, J.S., Balinger, A., Blumenkrantz, D., Calnan, D.P., Cramer, R., and Hsuan, J.J. (2003). Localization of a highly active pool of type II phosphatidylinositol 4-kinase in a p97/valosin-containing-protein-rich fraction of the endoplasmic reticulum. Biochem. J. *373*, 57–63.

Wu, E.L., Cheng, X., Jo, S., Rui, H., Song, K.C., Dávila-Contreras, E.M., Qi, Y., Lee, J., Monje-Galvan, V., Venable, R.M., et al. (2014). CHARMM-GUI Membrane Builder toward realistic biological membrane simulations. J Comput Chem *35*, 1997–2004.

Yang, J., Yan, R., Roy, A., Xu, D., Poisson, J., and Zhang, Y. (2015). The I-TASSER Suite: protein structure and function prediction. Nat. Methods *12*, 7–8.

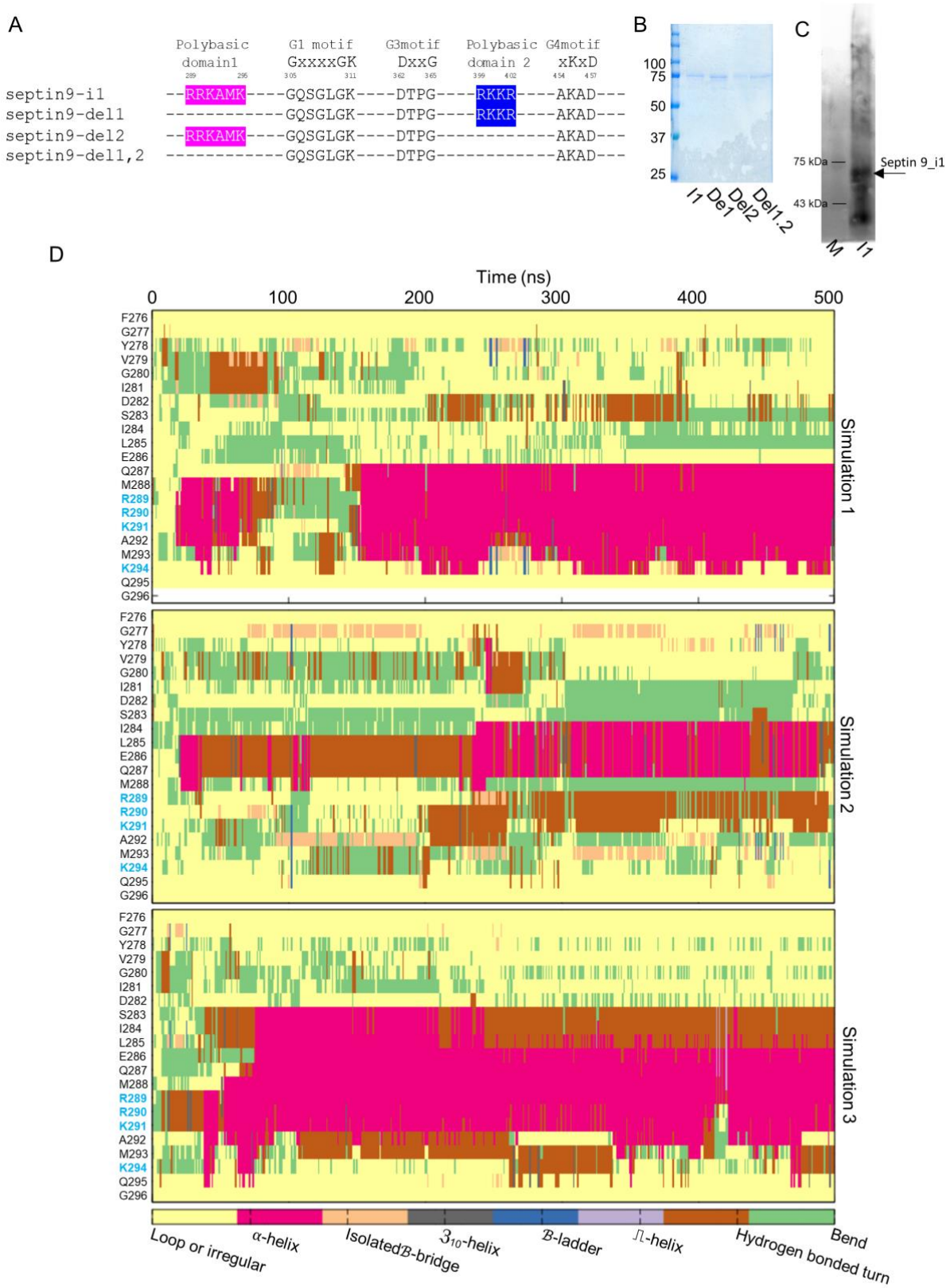
A
Polybasic domain1
G1 motif GxxxxGK
G3motif DxxG
Polybasic domain 2
G4motif xKxD
289 296 305 311 362 365 399 402 454 457
septin9-i1 --RRKAMK----GQSGLGK----DTPG----RKKR----AKAD---
septin9-del1 ----------GQSGLGK----DTPG----RKKR----AKAD---
septin9-del2 --RRKAMK----GQSGLGK----DTPG----------AKAD---
septin9-del1,2 ----------GQSGLGK----DTPG----------AKAD---
B
100
75
50
37
25
I1
De1
Del2
Del1.2
C
75 kDa
43 kDa
Septin 9_i1
M
I1
D
Time (ns)
0
100
200
300
400
500
F276
G277
Y278
V279
G280
I281
D282
S283
I284
L285
E286
Q287
M288
R289
R290
K291
A292
M293
K294
Q295
G296
Simulation 1
Simulation 2
Simulation 3
Loop or irregular
α-helix
Isolated β-bridge
3₁₀-helix
β-ladder
π-helix
Hydrogen bonded turn
Bend

Figure S1: Both PBs are required for septin 9_i1 assembly and the 21 residues towards N-terminal of PB1 folds in α-helix (Related to Figure 1)

A. Multiple alignment of septin 9_I1, septin 9_del1, septin 9_del2 and septin 9_del1.2 at polybasic domain 1(PB1), G-binding domain motifs G1, G3, G4, polybasic domain 2 (PB2).
B. Coomassie blue stained SDS–PAGE gel of purified septin 9_i1 and septin 9_del1, septin 9_del2 and septin 9_del1,2.
C. Western blot of native septin 9-I1 purified protein. In the M lane Conalbumine 75kDa and Ovalbumine 45kDa were separated as reference markers of the molecular weight.
D. Analysis of secondary structure of the N-terminal region peptide computed during 500 ns of MD simulations performed in triplicate (simulation 1 to 3).

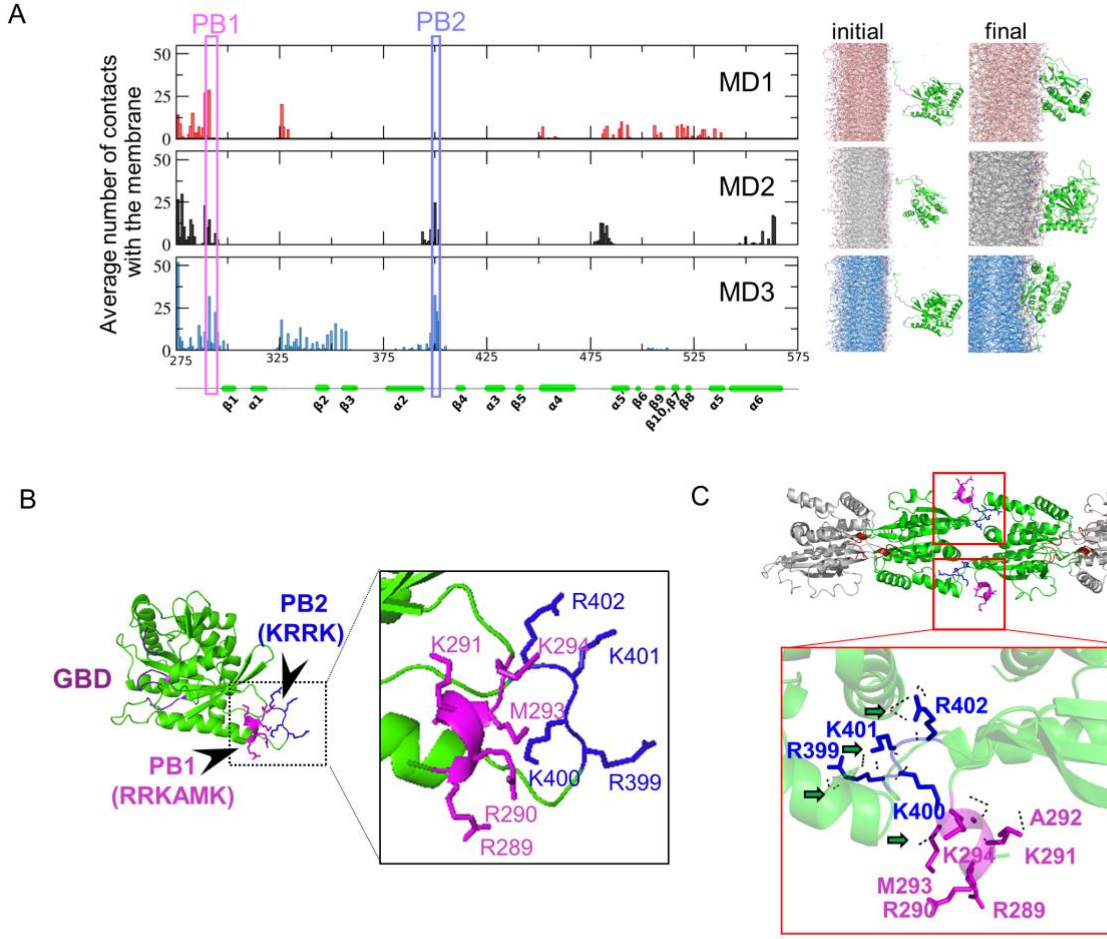
A
PB1
PB2
initial
final
Average number of contacts with the membrane
MD1
MD2
MD3
50
25
0
275
325
375
425
475
525
575
β1 α1 β2 β3 α2 β4 α3 β5 α4 α5 β6 β9 β10,β7 β8 α5 α6
B
GBD
PB2
(KRRK)
PB1
(RRKAMK)
R402
K291
K294
K401
M293
K400
R399
R290
R289
C
R402
K401
R399
K400
A292
K294
K291
M293
R290
R289
D
PtdIns(4)P(-)
PtdIns(4)P(+)
Protein sensibility to curvature
1,5
1
0,5
0
Septin9_i1
Septin 9_del1,2
E
Septin 9_del1
Septin 9_del2
Top
Bottom
PtdIns(4)P
Sonication
Top fraction %
100
75
50
25
0
liposome
large
small
PtdIns(4)P
Septin 9_del1
Septin 9_del2

Figure S2: PBs are required for septin 9_i1 PIs specific interaction and membranes form recognition (Related to Figure 2)

A. Three 100 ns long unbiased molecular dynamics simulating the interaction between human septin 9 monomer and a DOPC membrane. For each simulation (MD1, MD2 and MD3) the average of contacts with the membrane atoms that appeared during these simulations were counted and are shown as bar graphs. The right-side images show the conformation of the system at the beginning of the simulation and after the end of the simulation.
B. Homology modeling structural model of septin 9 monomer showing PB1 and PB2.
C. Homology modeling structural model of the septin 9 complex G9NC/NC9G. The two molecules of septin 9 on either side of the NC interface are shown in green, and their encompassed PB1 and PB2 are shown in magenta and blue, respectively. Squares indicate PB1 and PB2 shown at a higher magnification below. The residues for PB1 and PB2 are labeled. Green arrows indicate the salt bridges between PBs and neighboring septin 9.
D. Bar graph shows protein sensibility to curvature (ratio of pound prtein with small liposomes to that of big liposomes) dashed line indicate the 1value.
E. Left, western blots of the top and bottom fractions of septin 9_del1 (Del1) and septin 9_del2 (Del2) subjected to a liposome flotation assay; the arrow indicates the band corresponding to Septin9_i1 V5 tagged (68 kDa) further analyzed. Right, bar graph shows the percentage of protein in the top fraction (bound protein) from the analysis of the blots resulting from the liposome flotation assay.

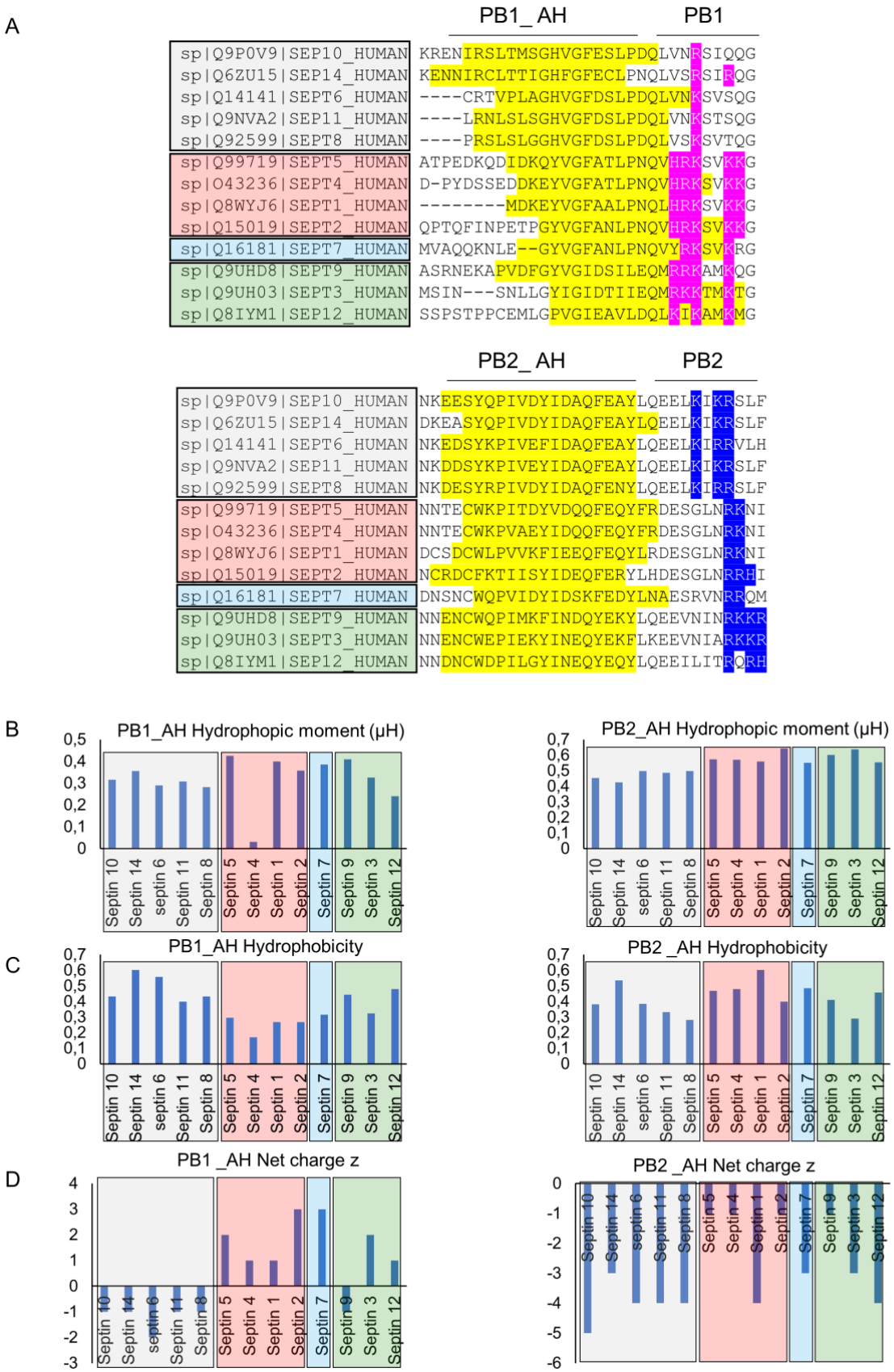
A
PB1_ AH
PB1
sp|Q9P0V9|SEP10_HUMAN KRENIRSLTMSGHVGFESLPDQLVNRSIQQG
sp|Q6ZU15|SEP14_HUMAN KENNIRCLTTIGHFGFECLPNQLVSRSIRQG
sp|Q14141|SEPT6_HUMAN ----CRTVPLAGHVGFDSLPDQLVNKSVSQG
sp|Q9NVA2|SEP11_HUMAN ----LRNLSLSGHVGFDSLPDQLVNKSTSQG
sp|Q92599|SEPT8_HUMAN ----PRSLSLGGHVGFDSLPDQLVSKSVTQG
sp|Q99719|SEPT5_HUMAN ATPEDKQDIDKQYVGFATLPNQVHRKSVKKG
sp|O43236|SEPT4_HUMAN D-PYDSSEDDKEYVGFATLPNQVHRKSVKKG
sp|Q8WYJ6|SEPT1_HUMAN --------MDKEYVGFAALPNQLHRKSVKKG
sp|Q15019|SEPT2_HUMAN QPTQFINPETPGYVGFANLPNQVHRKSVKKG
sp|Q16181|SEPT7_HUMAN MVAQQKNLE--GYVGFANLPNQVYRKSVKRG
sp|Q9UHD8|SEPT9_HUMAN ASRNEKAPVDFGYVGIDSILEQMRRKAMKQG
sp|Q9UH03|SEPT3_HUMAN MSIN---SNLLGYIGIDTIIEQMRKKTMKTG
sp|Q8IYM1|SEP12_HUMAN SSPSTPPCEMLGPVGIEAVLDQLKIKAMKMG
PB2_ AH
PB2
sp|Q9P0V9|SEP10_HUMAN NKEESYQPIVDYIDAQFEAYLQEELKIKRSLF
sp|Q6ZU15|SEP14_HUMAN DKEASYQPIVDYIDAQFEAYLQEELKIKRSLF
sp|Q14141|SEPT6_HUMAN NKEDSYKPIVEFIDAQFEAYLQEELKIRRVLH
sp|Q9NVA2|SEP11_HUMAN NKDDSYKPIVEYIDAQFEAYLQEELKIKRSLF
sp|Q92599|SEPT8_HUMAN NKDESYRPIVDYIDAQFENYLQEELKIRRSLF
sp|Q99719|SEPT5_HUMAN NNTECWKPITDYVDQQFEQYFRDESGLNRKNI
sp|O43236|SEPT4_HUMAN NNTECWKPVAEYIDQQFEQYFRDESGLNRKNI
sp|Q8WYJ6|SEPT1_HUMAN DCSDCWLPVVKFIEEQFEQYLRDESGLNRKNI
sp|Q15019|SEPT2_HUMAN NCRDCFKTIISYIDEQFERYLHDESGLNRRHI
sp|Q16181|SEPT7_HUMAN DNSNCWQPVIDYIDSKFEDYLNAESRVNRRQM
sp|Q9UHD8|SEPT9_HUMAN NNENCWQPIMKFINDQYEKYLQEEVNINRKKR
sp|Q9UH03|SEPT3_HUMAN NNENCWEPIEKYINEQYEKFLKEEVNIARKKR
sp|Q8IYM1|SEP12_HUMAN NNDNCWDPILGYINEQYEQYLQEEILITRQRH
B
PB1_AH Hydrophopic moment (μH)
PB2_AH Hydrophopic moment (μH)
C
PB1_AH Hydrophobicity
PB2 _AH Hydrophobicity
D
PB1 _AH Net charge z
PB2 _AH Net charge z
Septin 10
Septin 14
septin 6
Septin 11
Septin 8
Septin 5
Septin 4
Septin 1
Septin 2
Septin 7
Septin 9
Septin 3
Septin 12

Figure S3: Human septins have putative PB-associated amphipathic helices (Related to Figure 3)

A. Multiple alignments of 25 residues precedent to PB1 and PB2 in human septins. The sequences of the predicted amphipathic helices (AH) associated to PBs are highlighted in yellow.
B. Bar graph representing the hydrophobic moment generated by HeliQuest of the amphipathic helices highlighted in A.
C. Bar graph representing the hydrophobicity value generated by HeliQuest of the amphipathic helices highlighted in A.
D. Bar graph representing the net charge z value generated by HeliQuest of the amphipathic helices highlighted in A.

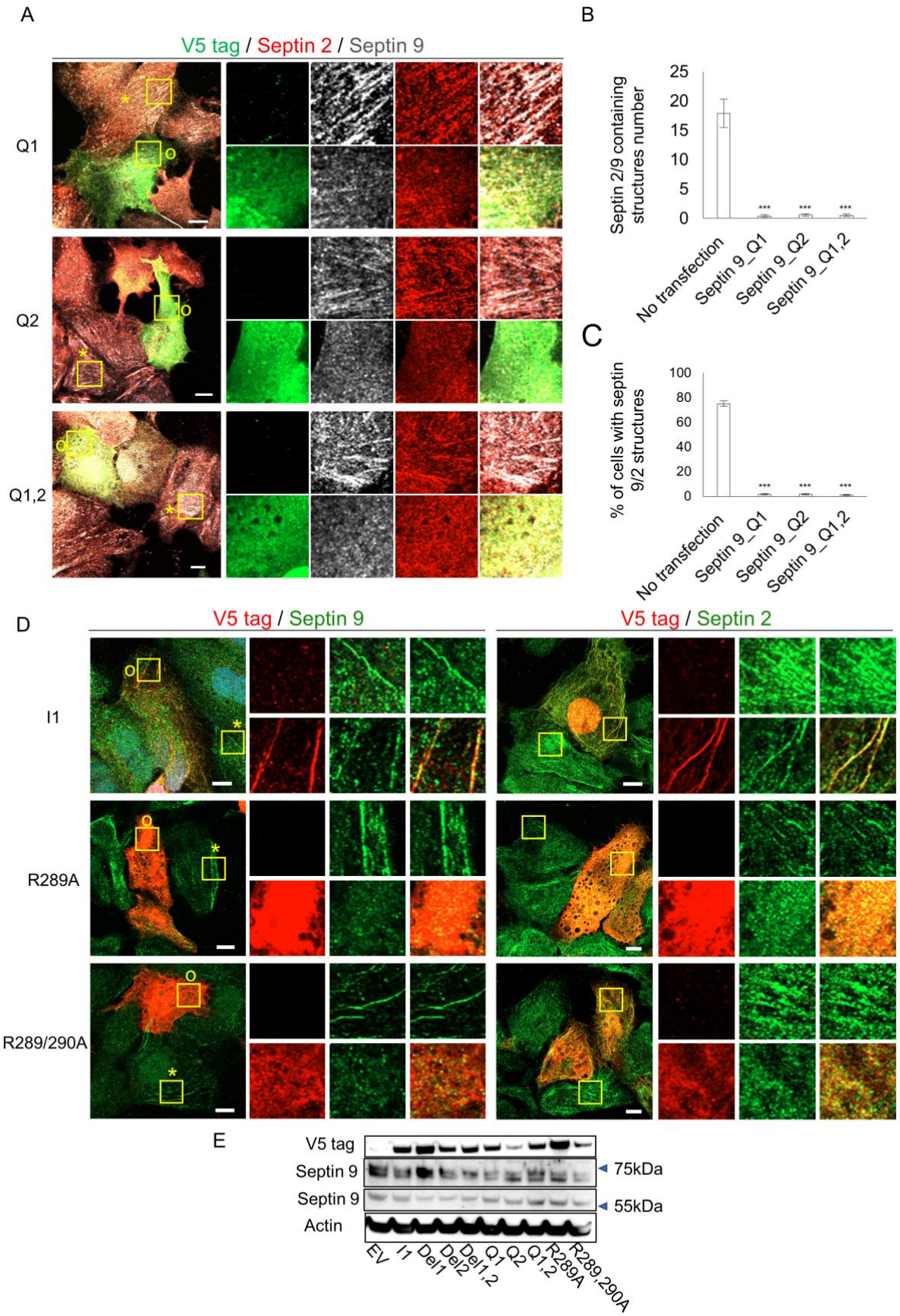
A
V5 tag / Septin 2 / Septin 9
Q1
Q2
Q1,2
B
Septin 2/9 containing structures number
25
20
15
10
5
0
***
***
***
No transfection
Septin 9_Q1
Septin 9_Q2
Septin 9_Q1,2
C
% of cells with septin 9/2 structures
100
80
60
40
20
0
***
***
***
No transfection
Septin 9_Q1
Septin 9_Q2
Septin 9_Q1,2
D
V5 tag / Septin 9
V5 tag / Septin 2
I1
R289A
R289/290A
E
V5 tag
Septin 9
Septin 9
Actin
75kDa
55kDa
EV
I1
Del1
Del2
Del1,2
Q1
Q2
Q1,2
R289A
R289,290A

Figure S4: Substitutional mutations of PBs domains have a similar effect to that of deletion mutation on septins filaments. (Related to Figure4)

A. Huh7,5 cells transfected with septin 9_Q1 (Q1), septin 9_Q2 (Q2) or septin 9_Q1,2 (Q1,2) for 48h, then fixed and stained for V5 tag (green), endogenous septin 2 (red) and endogenous septin 9 (grey). (*) indicates a low expression or not transfected cell and (0) indicates a transfected cell. Squares indicate the area shown at higher magnification to right.
B. Bar graph presenting the number of the filament structures of endogenous septin 9 and septin 2.
C. Bar graph representing the percentage of cells containing filament structures of endogenous septin 9 and septin 2.
D. Huh7,5 cells transfected with septin 9_i1 (I1), septin 9_R289A (R289A) or septin 9_R289/290A (R289/290A) for 48h, then fixed and stained for V5 tag (red), endogenous septin 2 (green) (left) and endogenous septin 9 (green) (right). (*) indicates a low expression or not transfected cell and (0) indicates a transfected cell. Squares indicate the area shown at higher magnification to the right.
E. Western blot analysis of endogenous septin 9 in huh7,5 cells transfected with septin 9_i1, septin 9_del1, septin 9_del2 septin 9_del1,2, septin 9_Q1 (Q1), septin 9_Q2 (Q2), septin 9_Q1,2 (Q1,2), septin 9_R289A (R289A) or septin 9_R289/290A (R289/290A). The tow detected bands (75kDa, 55kDa) by the antibody were presented.

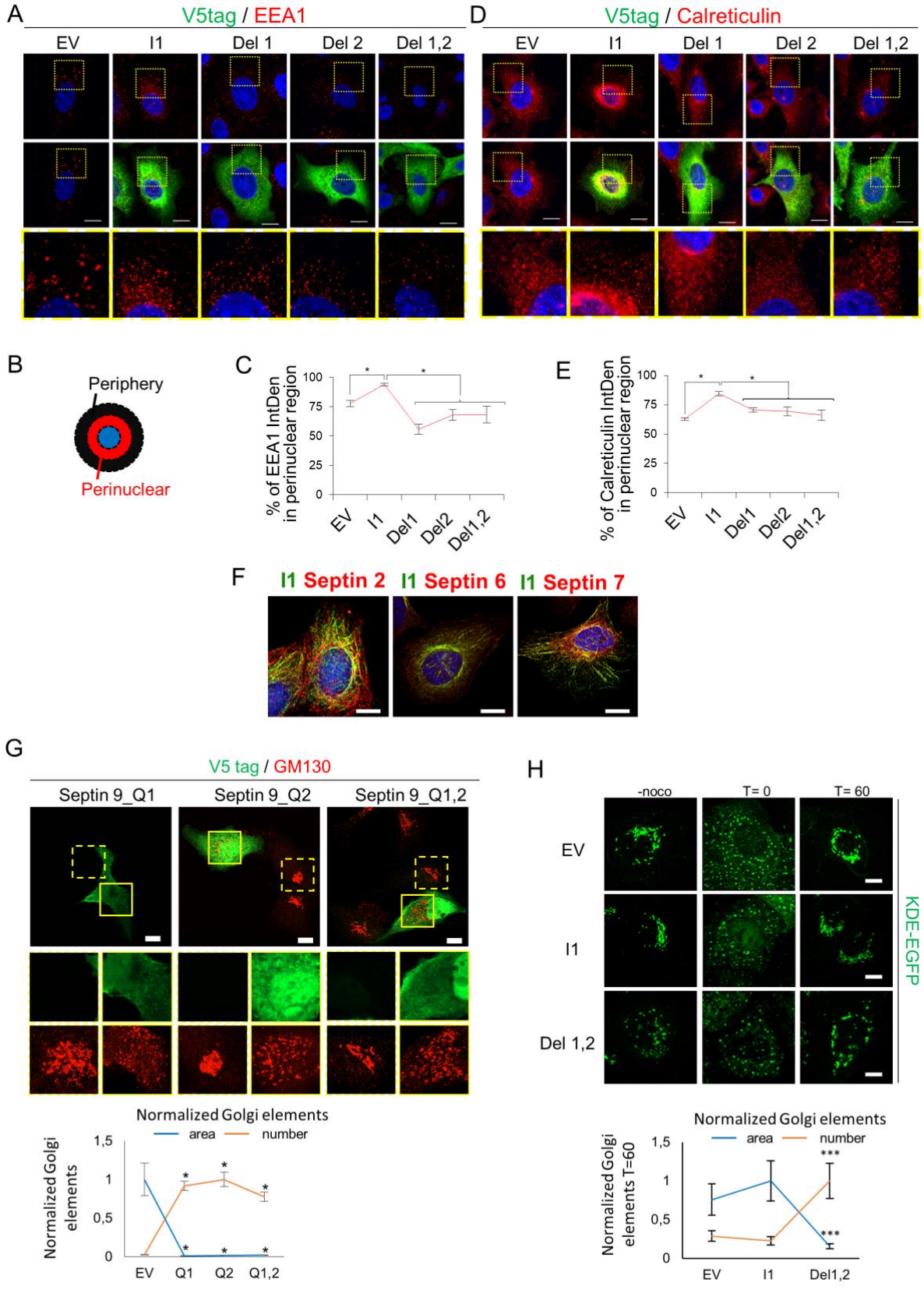
A
V5tag / EEA1
EV
I1
Del 1
Del 2
Del 1,2
D
V5tag / Calreticulin
EV
I1
Del 1
Del 2
Del 1,2
B
Periphery
Perinuclear
C
% of EEA1 IntDen in perinuclear region
100
75
50
25
0
EV
I1
Del1
Del2
Del1,2
E
% of Calreticulin IntDen in perinuclear region
100
75
50
25
0
EV
I1
Del1
Del2
Del1,2
F
I1 Septin 2
I1 Septin 6
I1 Septin 7
G
V5 tag / GM130
Septin 9_Q1
Septin 9_Q2
Septin 9_Q1,2
Normalized Golgi elements
area
number
Normalized Golgi elements
1,5
1
0,5
0
EV
Q1
Q2
Q1,2
H
-noco
T= 0
T= 60
EV
I1
Del 1,2
KDE-EGFP
Normalized Golgi elements
area
number
Normalized Golgi elements T=60
1,5
1
0,5
0
EV
I1
Del1,2

Figure S5: Mutated septin 9 i1 are incapable of having the effect of septin 9_i1 on Golgi, ER and EE compartments. (Related to Figure 5)

A. HeLa cells transfected with either empty vector (EV), septin 9_i1 (I1), septin 9_del1 (Del1), septin 9_del2 (Del2) or septin 9_del1,2 (Del1,2) for 48h, then fixed and stained for EEA1 (red) and V5tag (green). The dotted square indicates the area shown at higher magnification below. Scale bar: 10µm.

B. Representation of the peripheral (black) and perinuclear (red) regions of the cell.

C. Line graph representing the percentage of EEA1 in the perinuclear region from two experiments performed as described in A. The data are shown as mean ± SEM from 10 cells under each condition.

D. Cells transfected as described in (A) were stained for calreticulin (red) and V5tag (green). The dotted square indicates the area shown at higher magnification below. Scale bar: 10µm.

E. Bar graph representing the percentage of calreticulin in the perinuclear region from two experiments performed as described in a. The data is shown as mean ± SEM of 10 cells under each condition from two independent experiments.

F. HeLa cells transfected with septin 9_i1 for 48h then fixed and stained for V5tag (green) and septin 2 or septin 6 or septin 7 in red. Scale bar: 10µm.

G. Huh7,5 cells transfected with septin 9_Q1, septin 9_Q2, septin 9_Q1,2 for 48h the fixed and stained for GM130 (red) and V5tag (green). Scale bar 10. Line graph below representing normalized Golgi elements area and number. 10 cells were analyzed form tow independent experiments.

H. MDCK stably transfected with either EV, septin 9_i1 (I1) or septin_9 del1.2 (Del1,2) were transfected with KDE-GFP for 24h to visualize the Golgi. Cells were subjected to a nocodazole washout experiment. Scale bar: 10µm. Line graph below presents the normalized Golgi elements area and numbers calculated from 10 cells after 60 minutes of

nocodazole removal in two independent experiments. Student's t-test was used in C, E, G and I: *P<0.05, **P<0.001, ***P<0.0001.

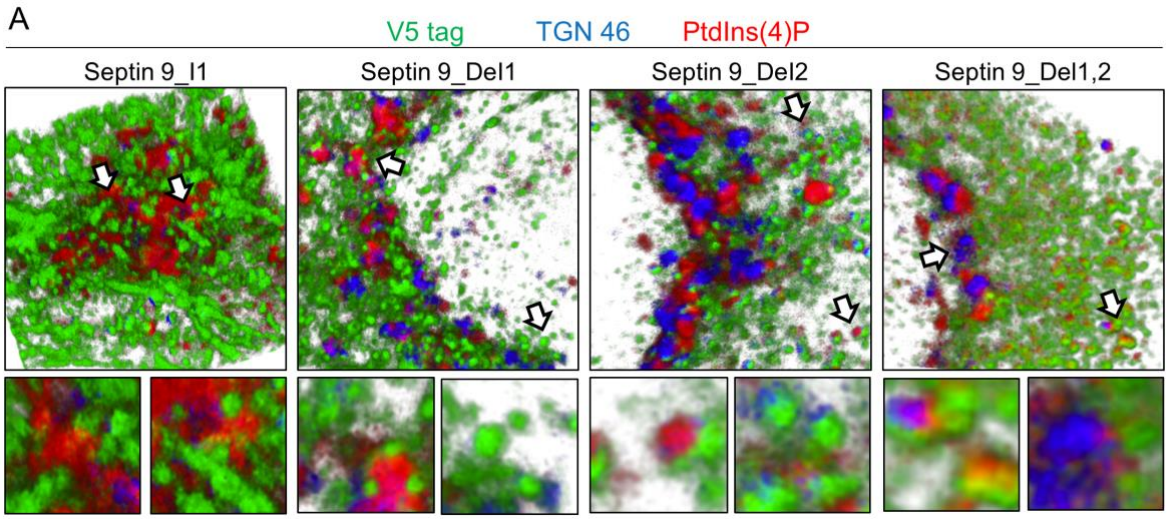
A
V5 tag
TGN 46
PtdIns(4)P
Septin 9_I1
Septin 9_Del1
Septin 9_Del2
Septin 9_Del1,2

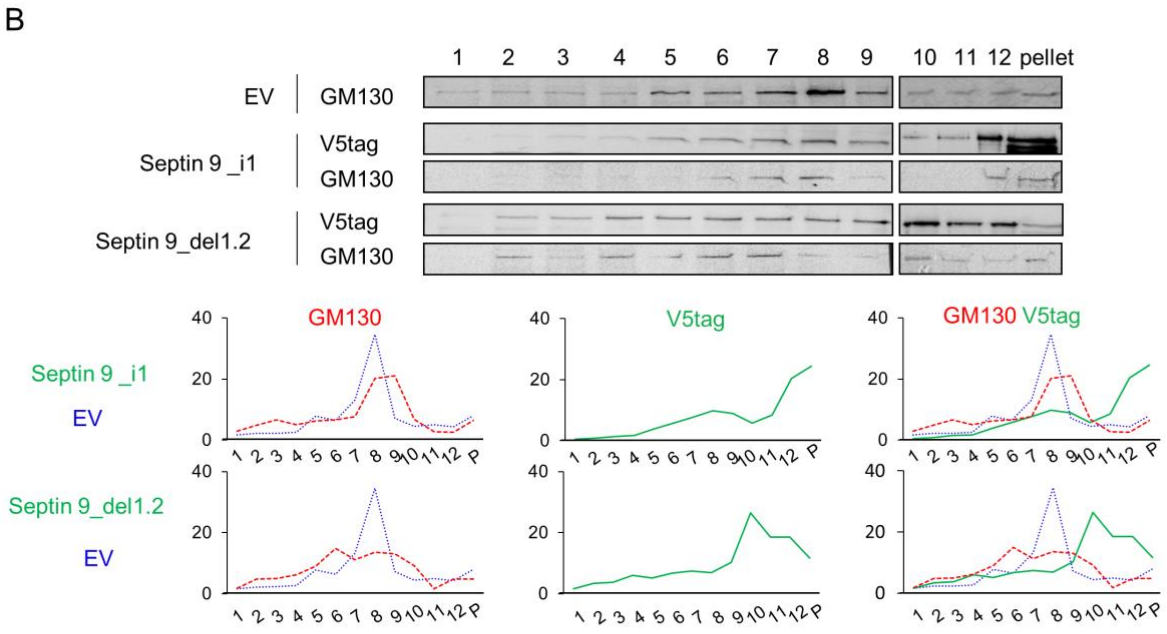
B
1 2 3 4 5 6 7 8 9 10 11 12 pellet
EV
GM130
Septin 9 _i1
V5tag
GM130
Septin 9_del1.2
V5tag
GM130
GM130
V5tag
GM130 V5tag
Septin 9 _i1
EV
Septin 9_del1.2
EV
40
20
0
1 2 3 4 5 6 7 8 9 10 11 12 P

Figure S6: Septin 9 is dispensable for PtdIns4P enrichment on Golgi and their PBs are required for specific recruitment to Golgi ((Related to Figure 6)

A. Images in Figure 6 panel (A) shown in 3D reconstruction with arrows indicating the area shown below at higher magnification. The zoomed in regions show example cases: in the septin mutants (green), the protein's signal either does not colocalizes with any of the PtdIns4P or GM130 signals (in red and blue respectively), or colocalize with only one of them, or with both.
B. MDCK EV, septin 9_i1 (I1) and septin 9_del1.2 (Del1,2) stably transfected cells were grown for 48h before being subjected to a subcellular fractionation assay and analyzed with Western blot for V5tag and GM130. The line graphs below show the densitometry analysis of the presented Western blots.

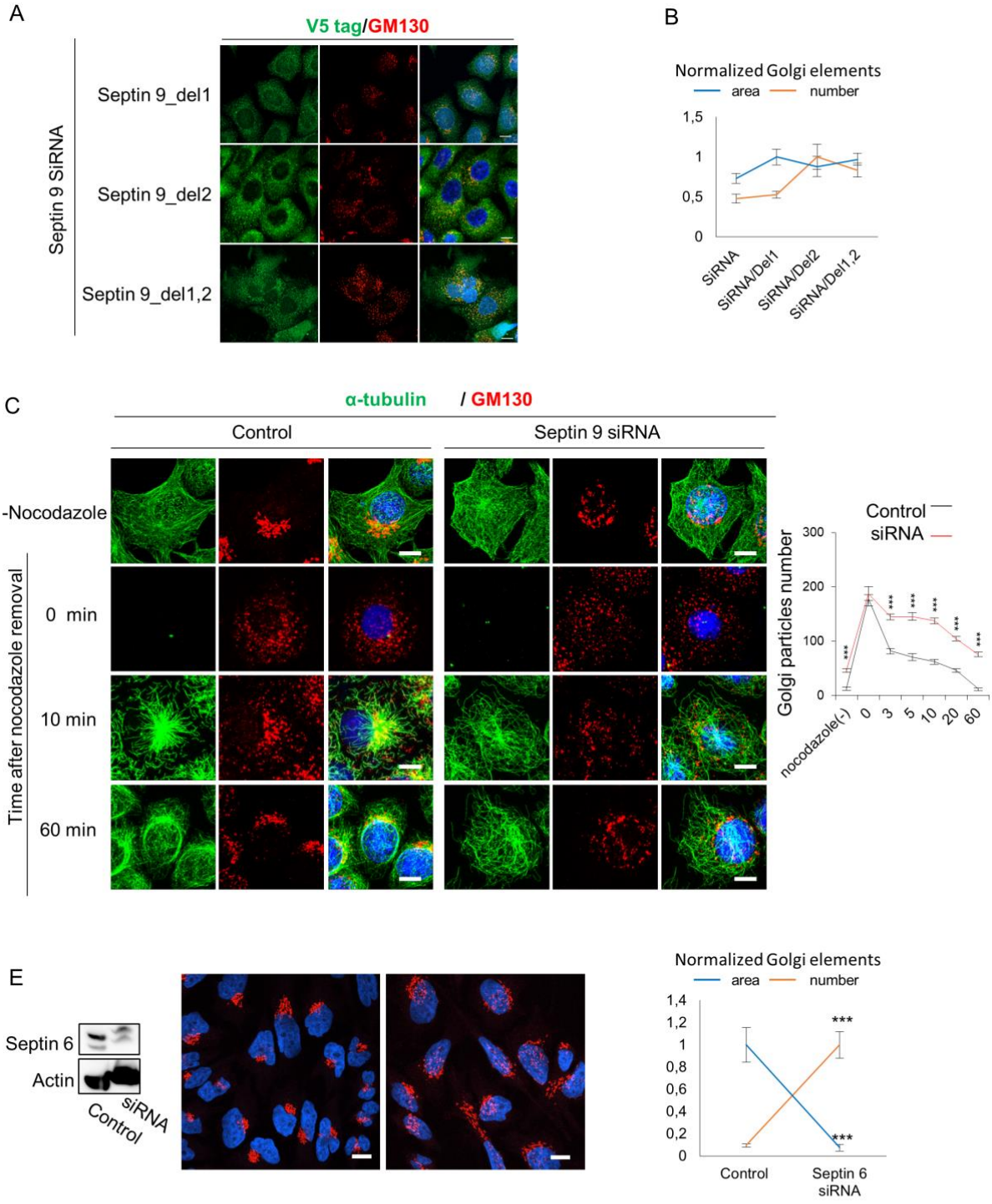
A
V5 tag/GM130
Septin 9 SiRNA
Septin 9_del1
Septin 9_del2
Septin 9_del1,2
B
Normalized Golgi elements
area
number
1,5
1
0,5
0
SiRNA
SiRNA/Del1
SiRNA/Del2
SiRNA/Del1,2
C
α-tubulin / GM130
Control
Septin 9 siRNA
-Nocodazole
Time after nocodazole removal
0 min
10 min
60 min
Control
siRNA
Golgi particles number
300
200
100
0
nocodazole(-)
0
3
5
10
20
60
E
Septin 6
Actin
siRNA
Control
Normalized Golgi elements
area
number
1,4
1,2
1
0,8
0,6
0,4
0,2
0
Control
Septin 6 siRNA

Figure S7: Septin 9 is required for Golgi assembly (Related to Figure 7)

A. septin 9 siRNA cells were transfected with septin 9_del1 (Del1), septin 9_del2 (Del2) or septin 9_del1,2 (Del1,2) for 48h and stained for GM130 (red) V5tag (green). Scale bar: 10µm.

B. Line graph representing the normalized area and number of Golgi elements in 15 cells from two independent experiments.

C. Septin 9siRNA and control cells were treated with nocodazole for 1 hour at 37°C and placed on ice for 2 hours. The cells were washed five times with ice-cold culture medium to remove the nocodazole and then moved to medium at 37°C for the time indicated in the Figure. The cells were then extracted, fixed and stained for αtubulin (green) and GM130 (red). Scale bar: 10µm. Line graph presenting the number of Golgi elements. Values are mean ± SEM of 30 cells from two independent experiments. Student's t-test was used ***P<0.0001.

D. HeLa cells transfected with septin 2 siRNA or septin 6 siRNA for 48h were analyzed by western blot (left) and confocal microscopy for GM130 (red) (middle). Scale bar: 10µm. Line graph presenting Golgi element's area and size. Values are mean ± SEM from 15 cells under each condition. Student's t-test was used ***P<0.0001.

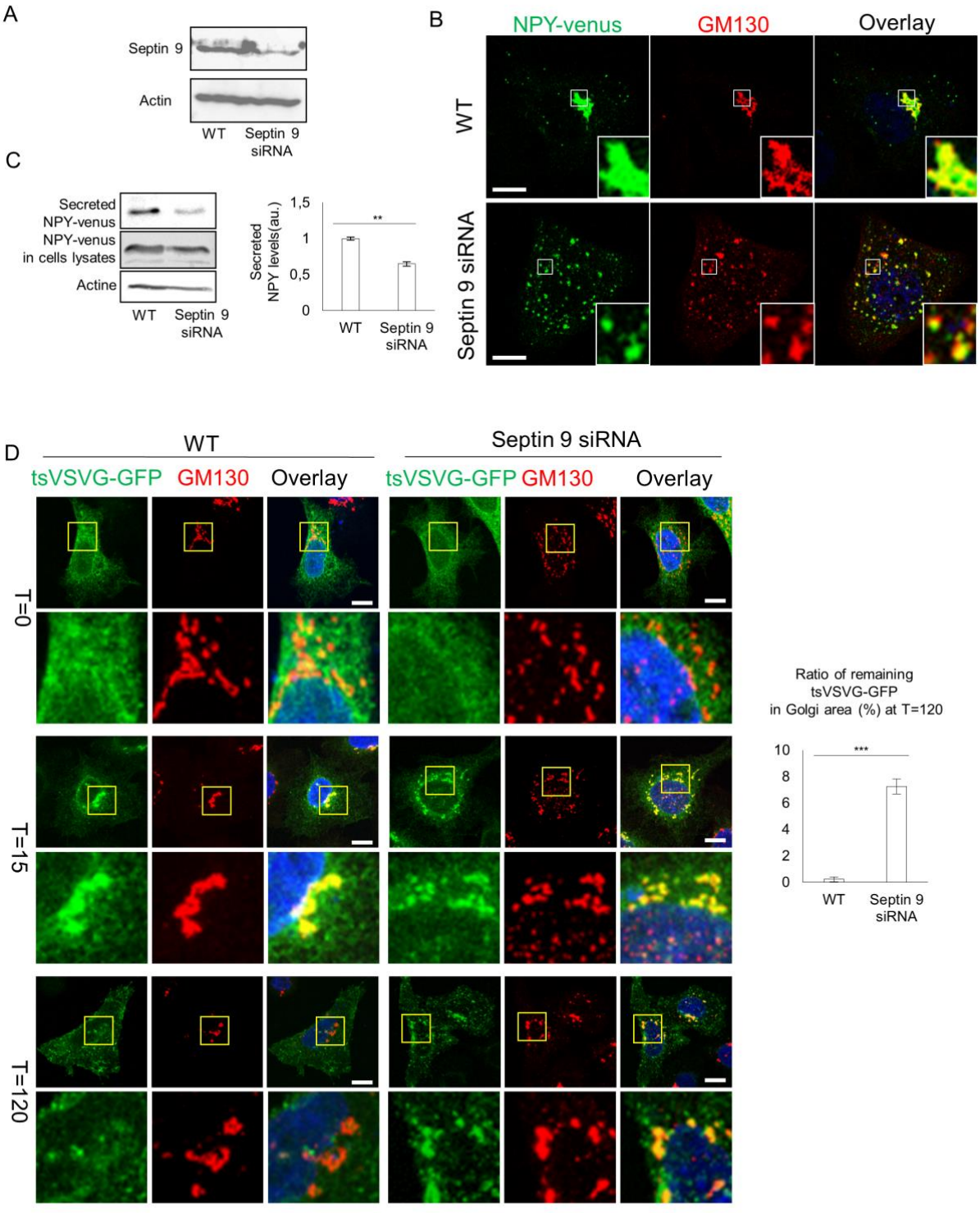
A
Septin 9
Actin
WT
Septin 9 siRNA
B
NPY-venus
GM130
Overlay
WT
Septin 9 siRNA
C
Secreted NPY-venus
NPY-venus in cells lysates
Actine
WT
Septin 9 siRNA
Secreted NPY levels(au.)
1,5
1
0,5
0
**
WT
Septin 9 siRNA
D
WT
Septin 9 siRNA
tsVSVG-GFP
GM130
Overlay
T=0
T=15
T=120
Ratio of remaining tsVSVG-GFP in Golgi area (%) at T=120
10
8
6
4
2
0
***
WT
Septin 9 siRNA

Figure S8. Septin 9 depletion affects Golgi morphology and intracellular transport (Related to Figure 7)

A. Immunoblot of septin 9 in septin 9 siRNA and control cells.

B. Control and septin 9 siRNA cells were transfected with NPY-venus for 24h prior to fixing and staining for GM130 (Red). Scale bar: 10µm.

C. Control and septin 9 siRNA cells were transfected with NPY-venus and incubated with the same culture volume for 24h. NPY-venus was analyzed by Western blotting in the culture medium and cellular lyses. The bar graph to the right representing the mean ± sem from three independent experiments. *P<0.05, (Student's t-test).

D. Septin 9 siRNA and control cells were transfected with tsVSVG-GFP and incubated at 37 °C for 3h and then at 40°C for a further 16h prior to being incubated at 32°C for the indicated time in the presence of 50 µg/ml cycloheximide. After incubation, the cells were fixed and stained for GM130 (red). Scale bar: 10µm. Bar graph representing the remaining tsVSVG-GFP in the Golgi area after 120 minutes of incubation at 32°C. N= 10 cells from two independent experiments.

Table S1. Mutagenesis primers sequence. (Related to Figure S1, Figure S4)

Pet21d septin 9_i1-F	CTCCGTCGACAAGCTATGAAGAAGTCTTACTCAGGAGG
Pet21d septin 9_i1-R	GGTGGTGGTGCTCGATCAATGGTGATGGTGATGAT
septin 9_del1 F	CATCCTGGAGCAGATGCAGGGCTTCGAGTTCA
septin 9_del1 R	TGAACTCGAAGCCCTGCATCTGCTCCAGGATG
septin 9_del2 F	GTCAACATCAACATCCCGGACACCCG
septin 9_del2R	CGGGTGTCCGGGATGTTGATGTTGAC
septin 9_Q1F	TCCTGGAGCAGATGCAGCAGCAGGCCATGCAGCAGGGCTTCGAGT
septin 9_Q1R	ACTCGAAGCCCTGCTGCATGGCCTGCTGCTGCATCTGCTCCAGGA
septin 9_Q2F	GAGGAGGTCAACATCAACCAGCAGCAGCAGATCCCGGACACCCGCGTCC
septin 9_Q2R	GGACGCGGGTGTCCGGGATCTGCTGCTGCTGGTTGATGTTGACCTCCTC
septin 9_R289AF	CCTGGAGCAGATGGCCCGGAAGGCCATG
septin 9_R289AR	CATGGCCTTCCGGGCCATCTGCTCCAGG
septin 9_R289/290AF	TGGAGCAGATGGCCGCGAAGGCCATGAAGC
septin 9_R289/290AR	GCTTCATGGCCTTCGCGGCCATCTGCTCCA